Available online at www.sciencedirect.com
SCIENCE DIRECT
ELSEVIER
International Journal of Solids and Structures 43 (2006) 3739–3769
INTERNATIONAL JOURNAL OF SOLIDS and STRUCTURES
www.elsevier.com/locate/ijsolstr

Towards a multiscale analysis of periodic masonry brickwork: A FEM algorithm with damage and friction

Giuseppina Uva [a,*], Ginevra Salerno [b]

[a] Department of Sciences of Civil Engineering and Architecture, Politechnical University of Bari, via Orabona n. 4, 70125 Bari, Italy
[b] Department of Structures, University of "Roma Tre", via Vito Volterra n. 62, 00146 Roma, Italy

Received 12 May 2005; received in revised form 2 June 2005
Available online 22 December 2005

Abstract

The aim of this paper is to present an effort towards a multiscale model of the inelastic behaviour of masonry brick panels and the relative solution algorithm. The essential features of the inelastic behaviour, such as the damage development within the bed joints and the frictional dissipation over cracks' faces, are taken into account. Micromechanical solutions are adopted in order to trace the guidelines for modelling the mentioned phenomena, and FEM analyses of large-scale panels are shown.

Keywords: Periodic masonry brickwork; In-plane behaviour; Damage and plasticity; Multiscale analysis; Homogenization; FEM analysis

1. Introduction

The mechanical behaviour of masonry structures is one of the most complex and challenging matters of the modern structural engineering. Indeed, masonry is a composite material, highly inhomogeneous and anisotropic because of the presence of mortar joints acting as weak points within the structure (Page, 1981; Syrmakezis and Asteris, 2001). The mechanical response, as a consequence, exhibits significant non-linear, irreversible and dissipative phenomena, which cannot be neglected by a structural model aimed at the prediction of the ultimate load and of the response under cyclical loads for masonry structures. The relevant mechanical phenomena that should be considered in order to describe the material behaviour (such as cracks' nucleation and growth within mortar layers or mortar–brick interfaces; frictional sliding at the contact between opposite cracks' faces; rocking of indented cracks edges) actually take place at a very small scale. On the other side, the structure is governed, in its peculiar overall response, by its global geometrical and morphological configuration. For instance, in masonry buildings the distribution of the loads among the different

* Corresponding author.
E-mail addresses: g.uva@poliba.it (G. Uva), salerno@uniroma3.it (G. Salerno).

0020-7683/$ - see front matter © 2005 Elsevier Ltd. All rights reserved.
doi:10.1016/j.ijsolstr.2005.10.004

structural elements is deeply influenced by the effectiveness of the box-like behaviour, whereas for historical masonry bridges, fundamental is the load path developed through the arc-effect.

In the early stages, the research studies developed in this field produced two different and antithetic visions, which for a long time have been the centre of a lively cultural debate within the scientific community (Hughes and Pande, 2001). On one side there was a continuous idea of masonry structures, in which the different structural elements (masonry piers, slabs,...) were modelled by means of classical continuous elements (plates, shells, panels,...) endowed with agile constitutive functions and then assembled in order to provide the final overall response of the structural system (Italian Ministry of Public Works, 1981). On the other side, a different approach was followed, by interpreting each of the constituents in the masonry assembly (i.e. each block and mortar joint) as an individual body, endowed with specific geometric and mechanical properties, and accordingly performing the analysis for the actual assemblage of elements (Hart et al., 1988).

Each of the two mentioned visions has indeed a high theoretical dignity and presents a number of advantages (among others things, we could recall the affordable computational cost for the first one, and the solid physical basis for the second one). However, when these two approaches are proposed as completely self-sufficient, they reveal irremediable defects. Actually, the one just possess the qualities the other is lacking of. In the last few years, the rigidity of such a dichotomy has been softening, and the scientific community has progressively realized that between the two antithetical extremes it is necessary to find a reasonable compromise, in order to avoid excessive computational efforts when facing real case studies, but endowing continuous approaches with a well-founded mechanical basis (Hughes and Pande, 2001; Sutcliffe et al., 2001; Asteris and Tzamtzis, 2003). The literature about this questions is really wide: some references are given in the bibliography of the paper, to which the reader is also addressed in order to find a more exhaustive state of the art review (Hughes and Pande, 2001; Asteris, 2003; Sutcliffe et al., 2001; Asteris and Tzamtzis, 2003; Kouznetsova et al., 2001; Kouznetsova et al., 2004; Kouznetsova et al., 2002; Kouznetsova, 2002; Massart, 2003).

Many modern modelling approaches and algorithms are actually continuous models enriched with a very deep micromechanical insight, and could be defined, in the wide meaning of the word, "multiscale" approaches according to Phillips (1998), that is to say, algorithms in which different scales of observation of the same physical phenomenon interact, exchanging information. It is our opinion that a reflection and discussion should be promoted about multiscale algorithms in order to precise, for instance, the theoretical relationships with research fields like non-linear homogenization or damage mechanics, in which a geometric link with lower scales is hiddenly kept every time that stabilizing procedures for the finite element are adopted, aimed at the sanitization of mesh dependency. The authors' idea of multiscale is presented in Salerno and Uva (2002) and is referred to the use of a hierarchic strategy in which a clear and precise definition is made both for the physical-mathematical models and for the scaling operators among different physical scales.

This paper does not completely belong to the philosophy presented in Salerno and Uva (2002) (whose effectiveness is actually still being tested), but nevertheless represents an effort in that direction, and in this sense should be intended the word "towards" mentioned in the paper title. The objective is not only to give a micromechanical foundation for the definition of the inelastic part of the constitutive response (i.e. Eshelby's solution), but also to allow the interaction of the macroscopic scale, which is characterized by the finite element discretization of an equivalent homogeneous body obtained through standard homogenization techniques (Sanchez Palencia, 1992; Suquet, 1983), with the lower scales, where the discontinuous nature of masonry is perceived, and the mathematical variables usually introduced to measure the damage level and the frictional sliding do assume a precise physical meaning. The idea is that in quasi-fragile materials like mortars, macroscopic non-linear phenomena are an effect of nucleation and growing of cracks at the microstructural level, and that a significant role is played by friction. A consistent micromechanical derivation of the constitutive prescription would lead to a law with internal damage variables, endowed with proper multisurface domains and flow rules (even non-associative). It is well known that the integration of such a constitutive law is quite cumbersome. In order to reduce algorithmic difficulties and to exploit at the best the advantages of the iterative arc-length strategy employed in the evolution path-following analysis, the constitutive law has been reformulated within a scheme of localization–updating–averaging consistent with the classical homogenization method. Indeed, the framework for a real multiscale algorithm is then outlined. The research that is here presented belongs to this general framework, and is focused on the in-plane behaviour of periodic masonry brickwork. The aim is to predict the structural response both under monotonical and cyclical loading condi-

tions with sufficient accuracy but reasonable computational costs. The fulfillment of this objective is to be realized through progressive steps. In a first stage, the following two simplifying assumptions are made: (i) Only bed joints are supposed to suffer decohesion and frictional sliding, head joints are completely neglected and blocks are considered as perfectly elastic; (ii) Nucleation and propagation of cracks is always considered as confined within a plane and governed by *opening* and *sliding* modes, that are supposed to be uncoupled (that is to say, dilatancy is not modeled). Of course, the description that is obtained is slightly rough, but the aim of our research work is to consolidate a numerical basis for the analysis, pointing out the direction for future developments. Some experimental and numerical tests solved by different authors (Anthoine et al., 1994; Lagomarsino et al., 1995; Raijmakers and Vermeltfoort, 1992; Lourenço et al., 1994) have been selected for testing the model and the performance of the numerical strategy.

The paper is organized as follows: Section 2 is entirely devoted to provide a theoretical foundation of the constitutive choices, within the spirit of Eshelby's micromechanical solution, completed by the classical Mohr–Coulomb law and by Griffith's criterion. Then, in Section 3 the theoretical model is re-formulated for the sake of the computational management and the algorithm solution is outlined. Finally, in Section 4 results are presented and compared with benchmarks. Conclusions follow.

2. Constitutive modelling

2.1. Preliminary remarks

The resistance of masonry buildings to horizontal actions and seismic input is usually considered very low and unreliable. Indeed, this belief must be somewhat incorrect, since many ancient buildings still survive today, although they had not been intentionally and consciously designed to face unexpectedly strong earthquakes.

In order to explain this fact, it should be remembered that a proper structural organization encourages the spatial behaviour and allows the distribution of actions to the proper supporting elements. This is the primary condition under which an optimum development of the shear strength and of frictional dissipation effects can occur. During a seismic shaking, an evolution of cracks takes place and consequently there is an increase in the energy dissipation related to frictional phenomena. The effect is the enhancement of structural ductility, and even a material intrinsically brittle like masonry can adjust itself to face stresses that would otherwise be too strong for it.

It is then evident that it is very important to devote attention to the non-linear and inelastic part of the constitutive law, in order to obtain a satisfactory representation of the behaviour of masonry-like materials. In front of the complexity briefly outlined, descriptions based upon a pure linear elastic framework (traditional elastic perfectly brittle model, no-tension model) are a drastic reduction.

Experimental research has pointed out that the constitutive behaviour of masonry is basically a softening one, characterized by a progressive crack growth and by degradation in stiffness and strength. Moreover, it has been definitely shown that the amount of inelastic deformations and hysteretic dissipation is not so negligible. All these irreversible and dissipative phenomena make the structural response anisotropic and history dependent, but at the same time allow the development of plastic resources and the dissipation of part of the energy related to seismic events. For all these reasons, aiming at reconstructing the post-critical, non-linear branch of the equilibrium path, we have decided to pay attention to the mechanics of the events occurring at the *microscopic scale*.

Before getting into the heart of the matter, it is necessary to spend a few words and point out that we are dealing with a complex phenomenon where the structural response is governed by spatial scales that are very different one from the other, and vary from the level of the single mortar joint to that of the whole wall. With this idea, we will distinguish three different scales that will be referred to as *macro*, *meso* and *micro* scales. At the *macroscopic* scale we see the continuum model of the masonry panel (obtained through a proper homogenization of the lower scales), whereas at the *mesoscopic* level we see a non-homogenous, discrete system, composed of bricks and mortar joints. At the *microscopic* scale we finally get inside the mortar joint, where the relevant micromechanical phenomena we are interested in (such as crack's growth and frictional sliding) can be observed.

2.2. The micromechanical approach

Nucleation and growth of cracks at the microscopic scale (with a possible development of contact friction on the cracks' faces) play a crucial role in the structural response of masonry panels and are to be accurately described.

Damage Mechanics is able to explain the deterioration occurring at the mesoscale, where the information about the microscopic complexity is lost. The effects of the evolution of microcracks can be recovered by using a continuum internal variable controlling the damage, whose definition and evolution should somehow keep trace of the micromechanics of the problem.

The basis on which the choice and definition of the internal variables is made is a micromechanical model for quasi-brittle materials proposed by Alpa and Gambarotta (1990), Gambarotta (1995), Gambarotta and Lagomarsino (1993), Gambarotta and Lagomarsino (1994b). In order to develop this model, a graduated approach is followed, starting from the solution of the simpler problem involving a single crack, and then progressively enriching it.

During the loading process, microdefects can grow up: by adopting the classical reference framework of the Fracture Mechanics, their propagation can be basically traced back to three "crack modes" (Fig. 1): (I) Opening mode; (II) Sliding mode; (III) Tearing mode. These phenomena are the reason for the apparent drop off in the stiffness and strength of the material. After choosing a proper reference elementary volume (REV), the effect of the development of a single plane, penny-shaped crack (denoted by the index i) immersed in an elastic matrix and having a generic orientation singled out by a normal versor $\mathbf{n}_i$ (Fig. 2) can be analysed as a boundary problem in which an external far stress field is assigned for the loading condition.

The starting point for solving such a boundary problem and obtaining the elastic state induced by the crack in the REV (displacement, strain and stress fields) is represented by the Eshelby solution of the ellipsoidal inclusion problem (Eshelby, 1968a,b). An infinite solid containing an ellipsoidal inhomogeneity and subjected to a remote stress field is considered. Remarkably, supposing that both the matrix and the inclusion are made of elastic and homogeneous materials, it turns out that the strain and stress fields inside the inclusion (and on the interface as well) are uniform. Furtherly, the solution fields averaged over the REV can be expressed as the sum of two terms: the state induced by the far stress imagining that the solid were homogeneous with elastic constants corresponding to the matrix, plus an "inelastic" correction due to the presence of the inclusion.

If the inclusion is actually a hole (that is to say, stress free), its displacement and strain fields, in particular on the boundary (where they are actually meaningful), can still be computed, and the expression of the fields induced in the REV keeps the same additive form as before.

Since a crack can be simply generated by properly collapsing one of the semi-axes of an ellipsoidal cavity, the particularization of the above mentioned results suggests the way for computing the displacements of the two opposite sides of the crack u_i^* and provides the expression for the strain field induced in the REV by the opening of the single crack.

Finally, by adding the contributions of all the cracks embedded in the REV (the assumption that microdefects do not interact one with the other allows to superpose elastic states), the overall inelastic contribution $\mathbf{E}^*$

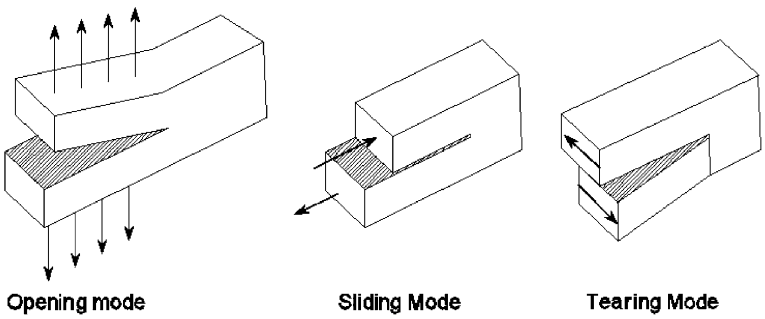

Fig. 1. Elementary crack propagation modes.

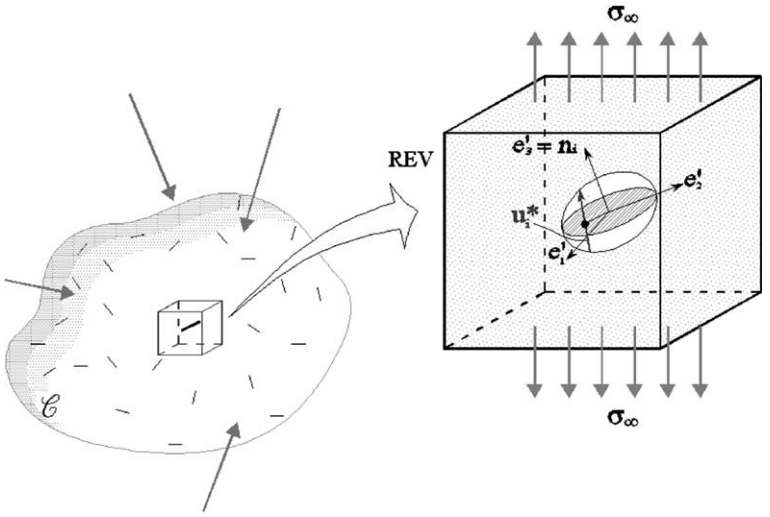

Fig. 2. A single microcrack immersed in the REV.

to the mesoscopic strain field $\mathbf{E}$ is evaluated ($\mathbb{C}$ compliance matrix; $\mathbf{n}_i$ normal versor to the plane of the ith crack, $\mathscr{N}$ total number of microcracks contained in the REV):

$$\mathbf{E} = \mathbb{C}\mathbf{T} + \mathbf{E}^* = \mathbb{C}\mathbf{T} + \sum_{i=1}^{\mathscr{N}} \left[\varepsilon_i^* \mathbf{n}_i \otimes \mathbf{n}_i + \mathrm{sym}\left(\boldsymbol{\gamma}_i^* \otimes \mathbf{n}_i\right)\right]. \tag{1}$$

According to the previous remarks, the inelastic contributions of the crack opening displacements to the mesoscopic strain field can be explicited by following the procedure sketched by Eshelby. It can be seen that they are a function of: the far stress solved in the crack plane ($\mathbf{t}_i = \mathbf{T}\mathbf{n}_i$), the mechanical parameters of the matrix, the geometry and the initial dimension of the crack (Budiansky and O'Connell, 1976; Hoenig, 1979; Hoenig, 1978; Nemat-Nasser and Horii, 1983). The "solved stress" can be split into two uncoupled components: $\mathbf{t}_i = \sigma_i \mathbf{n}_i + \boldsymbol{\tau}_i$, where $\sigma_i = \mathbf{T}\mathbf{n}_i \cdot \mathbf{n}_i$ and $\boldsymbol{\tau}_i = \mathbf{T}\mathbf{n}_i - \sigma_i \mathbf{n}_i$.

However, it is necessary to take into account the presence of the contact actions acting through the crack's faces (Fig. 3): in fact, the stresses applied to the crack plane can not be fully engaged for the crack's growth: at the beginning, the contact actions are opposed and dissipate by friction a part of the elastic energy of the external loads, that is no more available for the fracture propagation.

Hence, the solved stresses are turned into "effective stresses":

$$\begin{cases} \varepsilon_i^* = c_{\mathrm{n}i}\alpha_i \mathscr{H}(\sigma_i)\sigma_i = c_{\mathrm{n}i}\alpha_i \sigma_{i,\mathrm{eff}}, \\ \boldsymbol{\gamma}_i^* = c_{\mathrm{t}i}\alpha_i(\boldsymbol{\tau}_i + \mathbf{f}_i) = c_{\mathrm{t}i}\alpha_i \boldsymbol{\tau}_{i,\mathrm{eff}}. \end{cases} \tag{2}$$

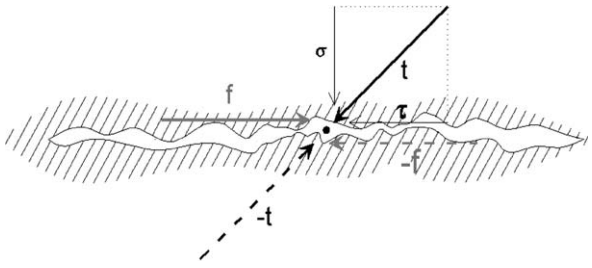

Fig. 3. Effective stresses over the crack's faces.

$\mathscr{H}(\cdot)$ = Heaviside step function: $\mathscr{H}(\cdot)=1$ if $\cdot>0$; $\mathscr{H}(\cdot)=0$ if $\cdot\leqslant 0$;
$\sigma_{i,\mathrm{eff}}=\mathscr{H}(\sigma_i)\sigma_i$;
$\boldsymbol{\tau}_{i,\mathrm{eff}}=(\boldsymbol{\tau}_i+\mathbf{f}_i)$;
$\mathbf{f}_i=-\boldsymbol{\tau}_i\mathscr{H}(-\sigma_i)=$ friction force; $\|\mathbf{f}_i\|-\mu\mid\sigma_i\mid\leqslant 0$;
$\mu=$ friction coefficient;
$c_{\mathrm{n}i}=$ normal compliance;
$c_{\mathrm{t}i}=$ tangential compliance.

Eshelby's solution in terms of effective stresses (2) depends also on the variable α_i, which is function only of the actual dimension of ith crack and assumes the role of *internal damage variable*, whose evolution will be followed during the loading process. The two mechanical parameters $c_{\mathrm{n}i}$ and $c_{\mathrm{t}i}$ are to be provided in the model.

Eq. $(2)_1$ shows that the normal strain ε_i^*, for a given α_i, is determined once the normal effective stress $\sigma_{i,\mathrm{eff}}$ is assigned. Actually, it is an unilateral constitutive constraint: the inelastic contribution vanishes if the crack is under a compression state, that is to say, if it is closed. In Eq. $(2)_2$ the friction is explicitly introduced in the form of the effective tangential stress $\boldsymbol{\tau}_{i,\mathrm{eff}}$. The presence of friction involves a problem of plasticity, and makes it necessary to keep a trace of the residual plastic tangential sliding, that becomes a further internal variable of the model: $\boldsymbol{\gamma}_{\mathrm{r}i}$.

The definition of the limit domains and the evolution laws for the internal variables α_i and $\boldsymbol{\gamma}_{\mathrm{r}i}$ is made according to the principles of Damage Mechanics (Krajicinovic, 1989; Krajicinovic and Fonseka, 1981; Lemaitre, 1984; Lemaitre, 1992). First of all, the static associated variables $\mathscr{G}_i$ and $\mathbf{f}_i$ (thermodynamic generalized forces) related to the internal variables should be defined, by means of the dissipated power $\mathscr{D}=-\mathbf{f}_i\cdot\dot{\boldsymbol{\gamma}}_{\mathrm{r}i}+\mathscr{G}_i\dot{\alpha}_i$. Trivially, the static variable associated to the residual plastic sliding $\boldsymbol{\gamma}_{\mathrm{r}i}$ is $-\mathbf{f}_i$. With regard to the damage state, the associated variable $\mathscr{G}_i$ can be defined according to the principles of Fracture Mechanics (Broek, 1984) as the energy release rate involved by the crack growth:

$$\mathscr{G}_i[\mathbf{t}_i,\alpha_i]=\left.\frac{\mathrm{d}w_{\mathrm{e}}[\mathbf{t}_i,\alpha_i]}{\mathrm{d}\alpha_i}\right|_{\mathbf{t}_i=\mathrm{cost}}=\frac{1}{2}\mathscr{H}(\sigma_i)\sigma_i\frac{\partial\varepsilon_i^*}{\partial\alpha_i}+\frac{1}{2}(\boldsymbol{\tau}_i+\mathbf{f}_i)\cdot\frac{\partial\boldsymbol{\gamma}_i^*}{\partial\alpha_i},\tag{3}$$

where w_{e} is the elastic strain energy stored in the REV in presence of the ith crack, characterized by the damage measure α_i, and under the constant stress state $\mathbf{t}_i$.

Now, it is necessary to properly choose some criteria governing the evolution of each α_i and the corresponding frictional sliding $\boldsymbol{\gamma}_{\mathrm{r}i}$. For the frictional sliding a classical Coulomb–Mohr law is adopted, while for the damage development an energetically based criterion is employed, following the approach suggested by Griffith. It is supposed that the propagation of a crack can take place when the energy released with the infinitesimal crack increment $\mathrm{d}\alpha_i$ (this is just the function $\mathscr{G}_i$ previously defined) becomes greater than the toughness $\mathscr{R}$ of the material, that is to say, the intrinsic strength opposed by the material to the crack growth (Broek, 1984):

$$\mathscr{G}_i[\mathbf{t}_i,\alpha_i]-\mathscr{R}[\alpha_i]\leqslant 0.\tag{4}$$

We will deal with a *concrete-like* material: according to Broek (1984), we will choose for it a toughness function containing all the meaningful features of the behaviour of a quasi-brittle material: an initial linearly elastic branch; a critical peak $(\alpha_{\mathrm{cr}},\mathscr{R}_{\mathrm{cr}})$; an unstable softening phase. The critical state defined by $(\alpha_{\mathrm{cr}},\mathscr{R}_{\mathrm{cr}})$ can be identified through uniaxial tests (pure tension or shear) on the material.

After all, the problem for a generic crack identified by α_i is expressed by the following system of plastic admissibility conditions and loading/unloading conditions:

$$\begin{aligned}
&\Phi_{\mathrm{d}i}[\mathbf{t}_i,\alpha_i]=\mathscr{G}_i-\mathscr{R}[\alpha_i]\leqslant 0\ \Rightarrow\ \frac{1}{2}c_{\mathrm{n}i}\mathscr{H}(\sigma_i)\sigma_i^2+\frac{1}{2}c_{\mathrm{t}i}\|\boldsymbol{\tau}_i+\mathbf{f}_i\|^2-\mathscr{R}[\alpha_i]\leqslant 0,\\
&\Phi_{\mathrm{s}i}[\mathbf{t}_i,\gamma_{\mathrm{r}i}]=\|\mathbf{f}_i\|-\mu|\sigma_i|\leqslant 0\ \Rightarrow\ \|\tau_i\|-\mu|\sigma_i|\leqslant 0,\\
&\Phi_{\mathrm{d}i}\dot{\alpha}_i=\dot{\Phi}_{\mathrm{d}i}\dot{\alpha}_i=0,\quad \dot{\alpha}_i\geqslant 0,\\
&\Phi_{\mathrm{s}i}\dot{\lambda}_i=\dot{\Phi}_{\mathrm{s}i}\dot{\lambda}_i=0,\quad \dot{\lambda}_i=0,\ \dot{\boldsymbol{\gamma}}_{\mathrm{r}i}=\mathbf{v}_i\dot{\lambda}_i,\ \mathbf{v}_i=-\frac{\mathbf{f}_i}{\|\mathbf{f}_i\|}.
\end{aligned}\tag{5}$$

For further details on the micromechanical model, the interested reader is addressed to the specific literature (Gambarotta and Lagomarsino, 1993; Gambarotta and Lagomarsino, 1994b).

The constitutive law defined by (5) is quite complex, and can be properly described within the framework of multisurface plasticity. The type of hardening occurring depends on the particular stress states: (1) pure tensile stress; pure shear; tension and shear; (2) compression and shear.

The first group of stress combinations is depicted in Fig. 4, where the evolution of the limit damage domains $\Phi_d[\alpha]$ for $0 < \alpha < \alpha_{cr}$ (top) and for $\alpha \geqslant \alpha_{cr}$ (bottom) is shown: for loading paths confined in the half-plane $\sigma \geqslant 0$, the material exhibits an isotropic hardening that is positive for $0 < \alpha < \alpha_{cr}$ and negative for $\alpha \geqslant \alpha_{cr}$. In the same figure, even if not active, the limit damage surfaces under compression are shown in the left shadowed half-plane and will be discussed later.

For fixed values of α, in the half–plane $\sigma \geqslant 0$ the limit curve is the semi-ellipse defined by the equation $\Phi_d^+[\alpha] = \frac{1}{2}c_n\sigma^2 + \frac{1}{2}c_t\|\boldsymbol{\tau}\|^2 - \mathscr{R}[\alpha] = 0$.

The second group of stress combinations (compression and shear—Fig. 5) is more complex. The simultaneous presence of shear and compression generates a frictional behaviour that is not merely governed by the Coulomb law. In fact, because of the interaction between plastic frictional sliding and damage, a combination of kinematical and isotropic hardening is triggered. With regard to the mathematical expressions, the damage domain $\Phi_d^-[\alpha] = \frac{1}{2}c_t\|\boldsymbol{\tau} + \mathbf{f}\|^2 - \mathscr{R}[\alpha_i] = 0$ in the half-plane $\sigma < 0$ is represented by two lines having a slope defined, respectively, by $-\mu$ and μ, and parallel to the classical Coulomb friction cone. Phenomenologically,

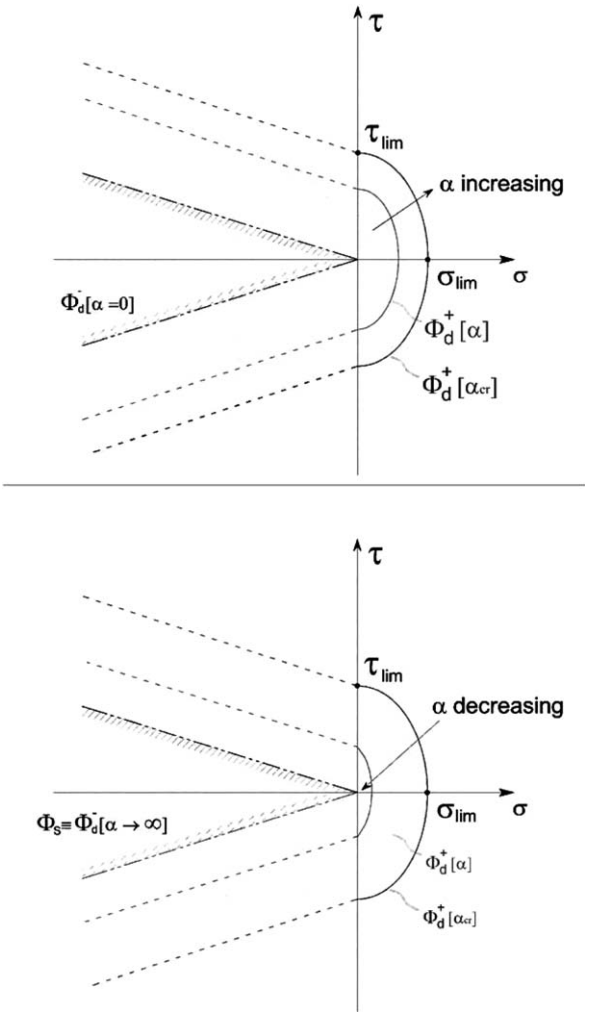

Fig. 4. Evolution of the limit domains for tension/shear loading paths: (a) $\alpha < \alpha_{cr}$, (b) $\alpha > \alpha_{cr}$.

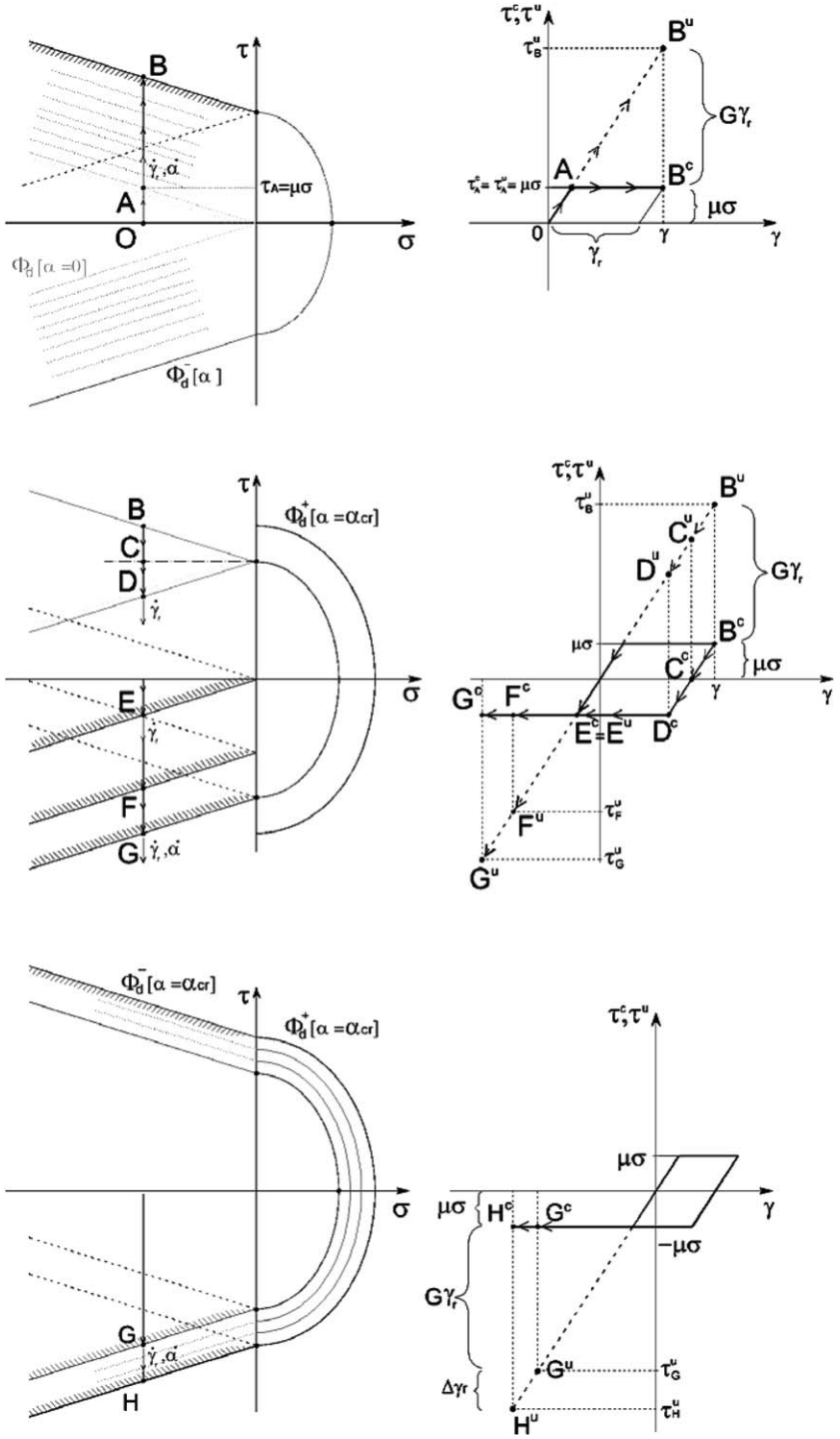

Fig. 5. Evolution of the limit domains for compression/shear loading paths.

the plastic sliding is actually bounded by the finite dimension of the crack and by the presence of the uncracked material fraction, so it can increase only when the crack dimension grows up.

In other words, this means that the damage limit domain and the frictional admissible surface are always linked on one side: every time that $\dot\alpha$ and $\dot\gamma_r$ are simultaneously positive, the limit damage surface is activated

and starts to expand ($\alpha < \alpha_{cr}$) or contract ($\alpha \geqslant \alpha_{cr}$), while a translation of the Coulomb cone (kinematical hardening) occurs. When $\dot{\gamma}_r < 0$, such an interaction is not activated, since $\dot{\alpha}$ is always non-negative: healing is not admitted by our damage model.

A further comment on Fig. 5 is useful for a better understanding of the constitutive model. In the left side of the figure, the actual mesoscopic stress state for the typical material point is represented in the stress domain (σ, τ). In the right side, instead, the different constitutive behaviour of the cracked fraction and of the uncracked one is traced in the plane (γ, τ) (the relevant quantities are denoted, respectively, with the superscripts "c" and "u"). This information, actually, is lost at the mesoscopic level and is here recalled in order to define the internal damage variable.

For each loading path in the mesoscopic stress domain (identified by capital letters), the corresponding plastic path for the cracked fraction (distinguished by capital letters with the superscript "c") can be read in the stress/strain domain. Also the "elastic" uncracked stress (superscript "u") is plotted in this graph, in correspondence of the actual value of the total tangential sliding γ.

Let us follow the loading path OAB/OAB^c shown in the top of Fig. 5. The line OA is characterized by a constant normal compression σ and by the closure of the crack because of friction: macroscopically, the behaviour is perfectly elastic. At point A, the initial limit surface is reached. The tangential stress τ becomes equal to $\mu\sigma$ (i.e., to the limit sliding threshold for the contact actions on the crack's surface). The Mohr–Coulomb constitutive law states that no increment of the tangential stress is possible on the cracked fraction: from now on (A–B), any additional external work will be entirely spent in the development of the inelastic sliding γ_r, while the microscopic tangential stress τ^c will remain frozen at the value $\mu\sigma$. Correspondently, an increment in the size of the crack's surface has to occur: together with the plastic sliding increment $\dot{\gamma}_r$, an increment $\dot{\alpha}$ takes place, and the limit domain consequently expands.

For example, at point B, the tangential stress of the cracked fraction τ^c is frozen at $\mu\sigma$ (B^c), while the inelastic sliding γ_r occurs. In the stress domain, this situation is represented by a vertical shifting of the initial cone, driven by the increments of both α and γ_r.

Now, if the representative stress point is driven back following the initial path and inverting the sign of the tangential stress (branch BCDEFG/B^{c}C^{c}D^{c}E^{c}F^{c}G^c in Fig. 5-middle), the cracked fraction undergoes the elastic unloading B^{c}C^{c}D^c until the microscopic stress τ^c attains the value $-\mu\sigma$. At this point (D/D^c), the development of a plastic sliding γ_r in the opposite direction starts. In the stress plane, all this happens within the instantaneous elastic domain, that is to say, with no increment of the internal variable α: there is a "free" space within which the sliding of the crack can take place at no extra-cost in terms of damage increase.

At the point G/G^c, the plastic sliding γ_r previously accumulated is completely recovered, and a further progress can only proceed if the crack's size accordingly grows up: $\dot{\gamma}_r > 0$ and $\dot{\alpha} > 0$. So, for example, the path GH/G^{c}H^c (Fig. 5-bottom) is characterized by the gain of a negative inelastic sliding $\Delta\gamma_r$ and by a new expansion of the limit damage surface, measured by $\Delta\alpha$.

2.3. Continuum modelling of masonry brickwork

As stated at the beginning, in order to avoid excessive computational costs, a macromodelling approach has been here adopted: instead of describing in detail the texture of a masonry panel, an equivalent Cauchy continuum has been defined, and its ideal mechanical properties have been obtained starting from those of its constituents. This operation is fulfilled by considering the masonry as made up of alternate layers of brick and mortar (Fig. 6b) and by homogenizing (Fig. 6c) this layered composite by standard techniques (Anthoine, 1994).

Head joints are neglected, although they are present in the initial topology (Fig. 6a), and this has allowed us to consider the homogenized continuum as transversely isotropic rather then orthotropic, at least in the elastic state. This could seem quite a rough assumption; however, the observation of existing structures and experimental testing seems to suggest that their influence plays only a secondary role in collapse mechanisms: ruptures are mostly localized in mortar bed joints (whose thickness is usually very small with respect to the other dimensions), at the contact surface between mortar and blocks rows, whereas the propagation of cracks more significantly involves bed joints (with the characteristic diagonal pattern) only in the late post-critical branch.

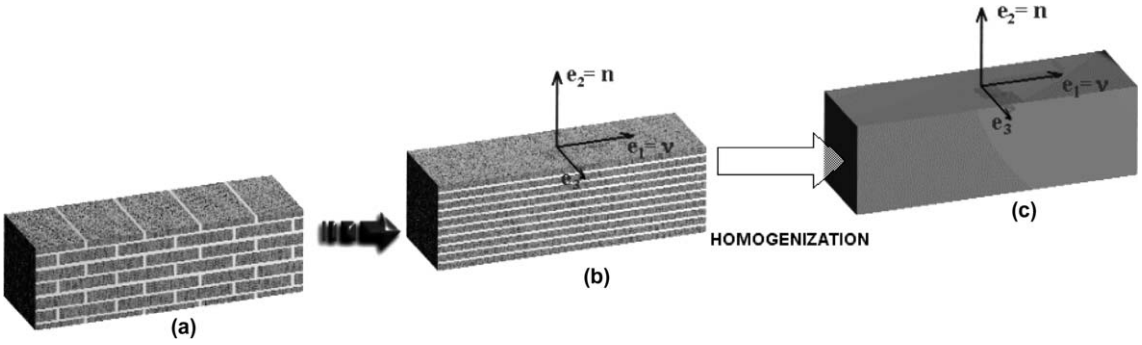

Fig. 6. Homogenization of the masonry panel seen as a transversely isotropic composite.

The micromechanical model briefly sketched in the previous paragraph can be fruitfully used for the modelling of masonry panels, as it was shown by some authors (Gambarotta and Lagomarsino, 1994a; Gambarotta et al., 1995). Of course, further simplifications will have to be introduced, if we do not want to loose sight of the practical exigencies of the analysis, aimed at the solution of large structures. Hence, before homogenizing, some additional hypotheses will be done.

First of all, we have chosen to deal with *plane* systems, and to focus the attention only on their *in-plane behaviour*. It is then supposed that the rupture within the horizontal mortar joints can only take place along an "interface" plane, whose position within the thickness of the bed is unimportant to the aim of the overall analysis. Hence, microcracks are described as a set of equi-oriented segments laying on the interface plane and governed by a unique scalar measure of damage, in the form of an internal variable controlling the cracks' length. Hence, from now on, the subscript i will be left out.

One more consequence is that the nucleation and propagation of cracks is only governed by opening and sliding elementary modes, supposed to be uncoupled (that is to say, dilatancy cannot be modelled). Actually, damage affects also the bricks, but in the proposed model this will be completely neglected: indeed the experimental evidence shows that it becomes significant only when a high compression state is attained (usually in the late post-critical branch, Ballio et al., 1993).

According to these assumptions, the micromechanical model (1) and (2) assumes a very simple form: only one scalar damage variable is introduced in each material point, able to account for the damage of the bed joints, whereas the bricks are supposed to remain elastic throughout all the loading process. During the loading process, the microdefects within the mortar interfaces split open—according to the opening mode and sliding mode (Section 2.2)—and are subjected to contact actions as a consequence of the harshness of the cracks' faces. As an effect of these mechanisms, inelastic deformations arise (Eq. (2)) and contribute to the macroscopic strain field $\mathbf{E}$ (Eq. (1)) of the equivalent continuum. In the elastic phase, the global response is described by the compliance matrix obtained by homogenizing the layered composite into a linear elastic transversely isotropic Cauchy material. In Fig. 6, axis 2 is the transverse isotropy axis. In the plane case, only four independent constants appear in the constitutive elastic coefficient matrix, that is, E_1, E_2, v and G:

$$\begin{Bmatrix} \varepsilon_1 \\ \varepsilon_2 \\ \gamma \end{Bmatrix} = \begin{bmatrix} \frac{1}{E_1} & -\frac{v}{E_1} & \cdot \\ -\frac{v}{E_1} & \frac{1}{E_2} & \cdot \\ \cdot & \cdot & \frac{1}{G} \end{bmatrix} = \begin{Bmatrix} \sigma_1 \\ \sigma_2 \\ \tau \end{Bmatrix}, \tag{6}$$

$$\begin{Bmatrix} \sigma_1 \\ \sigma_2 \\ \tau \end{Bmatrix} = \begin{bmatrix} E_1 + \frac{v^2}{\left[\frac{1}{E_2}-\frac{v^2}{E_1}\right]} & \frac{v}{\left[\frac{1}{E_2}-\frac{v^2}{E_1}\right]} & \cdot \\ \frac{v}{\left[\frac{1}{E_2}-\frac{v^2}{E_1}\right]} & \frac{1}{\left[\frac{1}{E_2}-\frac{v^2}{E_1}\right]} & \cdot \\ \cdot & \cdot & G \end{bmatrix} = \begin{bmatrix} St_{11}^E & St_{12}^E & \cdot \\ St_{12}^E & St_{22}^E & \cdot \\ \cdot & \cdot & St_{33}^E \end{bmatrix} = \begin{Bmatrix} \varepsilon_1 \\ \varepsilon_2 \\ \gamma \end{Bmatrix}, \tag{7}$$

where the stiffness coefficients St_{ij} are defined, and E_1, E_2, v and G assume the following form in terms of mortar and bricks elastic moduli (E_m, E_b, G_m, G_b) and of their volume fractions (η_m, η_b):

$$\begin{aligned} E_1 &= \eta_m E_m + \eta_b E_b, \\ v &= \eta_m v_m + \eta_b v_b, \\ E_2 &= \frac{1}{\dfrac{\eta_m v_m^2 + \eta_b v_b}{E_1} - \dfrac{\eta_m v_m^2}{E_m} + \dfrac{\eta_b v_b^2}{E_b} + \dfrac{\eta_m}{E_m} + \dfrac{\eta_b}{E_b}}, \\ G &= \frac{G_m G_b}{\eta_m G_b + \eta_b G_m}. \end{aligned} \tag{8}$$

Let us now homogenize the anelastic contribution. The REV will be chosen in order to contain just one bed joint. In that case, and considering that the tangential strain has only one component, the inelastic deformation in Eq. (1), only dependent on mortar bed joints, is specified as follows:

$$\mathbf{E}_m^* = \varepsilon_m^* \mathbf{n} \otimes \mathbf{n} + \gamma_m^* \boldsymbol{v} \otimes \mathbf{n} \begin{cases} \varepsilon_m^* = c_n \alpha \mathscr{H}(\sigma)\sigma; \\ \gamma_m^* = c_t \alpha(\tau + f); \end{cases} \quad \alpha = \sum_{i=1}^{\mathscr{N}} \alpha_i. \tag{9}$$

The notations and parameters used are the same introduced in Section 2.2, specifying that the material is the mortar. In particular, c_n and c_t are the normal and tangential compliance parameters governing the crack opening in the mortar bed joints.

The overall strain field in the masonry (variables referring to the homogenized masonry have been denoted with the index M), after the Reuss homogenization, becomes:

$$\mathbf{E}_M = \mathbb{C}_M \mathbf{T}_M + \eta_m \mathbf{E}_m^*. \tag{10}$$

Actually, while homogenization techniques for periodic media have been extensively and successfully applied in linearized elasticity, when the constituents are endowed with a non-linear behaviour there are not widely accepted and firmly stated homogenization procedures, and only in very simple cases, like this, it is possible to obtain a closed form for the solution.

3. Computational model

3.1. Preliminary remarks

Until now, an effort has been done in order to provide a preparatory theoretical background for the following analysis. The result is condensed in Eq. (9), that defines the constitutive law for the material "masonry". This formula actually describes a material that, after the homogenization procedure, is homogeneous everywhere except for a set of extremely localized inelastic singularities.

A natural procedure for the analysis could be, at this point, to write the incremental constitutive law starting from (9) and (5), and to integrate them with a standard predictor–corrector algorithm. Nevertheless, it is all the same natural to exploit the apriori knowledge about the geometrical position of the points where inelastic phenomena happen.

The selected theoretical model assumes that such inelastic events are localized within the mortar joints: it is then natural and wise, when performing a discretized numerical analysis, to place the sampling points just there. Since the chosen discretization method is a FEM one, this leads us to adjust the mesh so that the Gauss integration points lie within the mortar bed joints (Fig. 7). Furthermore, since these points are the place where the most relevant mechanical phenomena occur, not only they will be the sampling points for the stress state, but also they will provide the updated values of the internal variable, keeping the memory of the inelastic events.

On this subject, it is now worth spending some words about the opportunity of performing a "downscaling" into the micromechanics, in order to have a more conscious and less empirical control over the evolution of the internal variables. Such a scale switching is performed by applying a Voigt homogenization

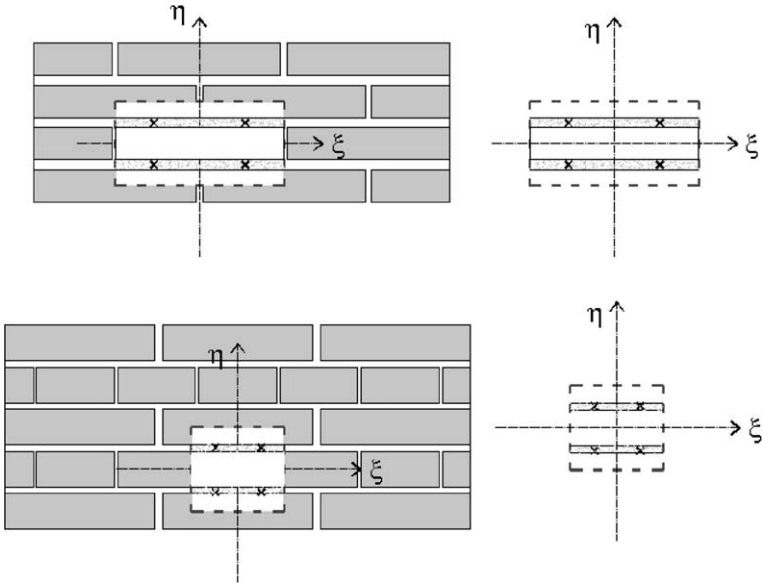

Fig. 7. Location of the sampling-Gauss points within the FEM discretization for two different masonry patterns.

just at each Gauss point, that becomes the doorway for a "material" universe (Fig. 8), where we try to discern within the complessity of microcracking in order to simplify it.

Let us look at Fig. 8. In a REV centered at the generic Gauss-point P we can imagine a horizontal surface on which microcracking phenomena are localized. Let A be the area of that surface, A^{c} be the total area of the cracks and $A^{\mathrm{u}} = A - A^{\mathrm{c}}$ be the area of the uncracked zone. Whatever is the distribution of the microcracks on that surface, the *first hypothesis* is to merge them in order to create two rectangular separate but contiguous subregions, both as deep as the REV itself. Let β be the "measure" of microcracks, defined as the ratio of the cracked area A^{c} with respect to the total area A. According to the first hypothesis, in a planar view, β

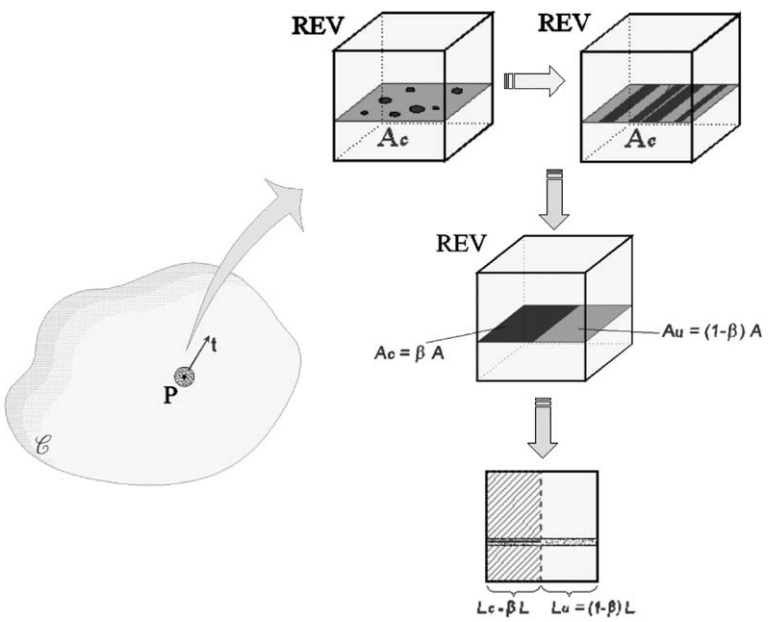

Fig. 8. The typical cracked material point as a system reacting in parallel: Voigt homogenization.

represents also the cracked fraction of the joint with respect to its total length (see always Fig. 8) and since the problem is now plane, it detects two plane subregions Ω^{u} and Ω^{c} whose union $\Omega = \Omega^{u} \cup \Omega^{c}$ is the plane REV. It is hardly worth noting that the ratio between the areas of Ω^{c} and Ω is β.

The *second hypothesis* imposes a uniform stress state in Ω^{u} and Ω^{c}: in particular, in Ω^{u} the stress state is indefinitely elastic, while in Ω^{c} it is practically equal (except for the σ_1 component) to the tension transmitted through the crack's faces into unilateral frictional contact (Uva, 1998). From these two hypotheses, it comes out that the contribution of microstress in the Gauss-point is weighted by β for the "cracked" zone and by $(1-\beta)$ for the "uncracked" zone.

Some words should be spent on Voigt's homogenization method, which is strictly related to the displacement formulation of Riks' step-by-step algorithm used to integrate the equilibrium equation system. In the generic iteration, given the displacements and the deformations compatible with them, the stress state is then calculated. Therefore, in the Gauss-point gateway the input is the strain, and the output is the stress. Voigt's homogenization is naturally fit for such an algorithmic hierarchy, because the down-scaling (localization operator) is governed by the strain, while the up-scaling (the average operator) is expressed in terms of stress.

3.2. Voigt homogenization

As pointed out, the internal variable governing the damage development in each monitored point is β, defined by:

$$\beta = \frac{A^{c}}{A} = \frac{L^{c}}{L} \rightarrow 1-\beta = \frac{A^{u}}{A} = \frac{L^{u}}{L}. \tag{11}$$

At each instant of the loading history, this internal variable, while identifying the ratio between the amount of cracked material and uncracked one, governs up and down scalings into the micromechanics of the joint.

Let now $\mathbf{E}_M$, $\mathbf{T}_M$ be respectively the strain and the stress tensors for the homogenized Cauchy material, $\mathbf{E}^{c}_M, \mathbf{T}^{c}_M$ the strain and the stress tensors for the cracked fraction, and, finally, $\mathbf{E}^{u}_M, \mathbf{T}^{u}_M$ the strain and the stress tensors for the uncracked fraction. The homogenization procedure is based on the equality of micro and macroworks (Hill's condition), under the same micro and macrostrains (Voigt's procedure), that is:

$$\int_{\Omega} \mathbf{T}_M \cdot \mathbf{E}_M = \int_{\Omega^{u}} \mathbf{T}^{u}_M \cdot \mathbf{E}^{u}_M + \int_{\Omega^{c}} \mathbf{T}^{c}_M \cdot \mathbf{E}^{c}_M, \quad \forall \mathbf{E}^{u}_M = \mathbf{E}^{c}_M = \mathbf{E}_M. \tag{12}$$

By performing (12), we obtain first:

$$\int_{\Omega} \mathbf{T}_M = \int_{\Omega^{u}} \mathbf{T}^{u}_M + \int_{\Omega^{c}} \mathbf{T}^{c}_M.$$

Then, by considering the averaged values and taking into account (11), we have:

$$\mathbf{T}_M = (1-\beta)\mathbf{T}^{u}_M + \beta \mathbf{T}^{c}_M. \tag{13}$$

In the basis drawn in Fig. 6, the components of the tensors $\mathbf{T}_M$, $\mathbf{T}^{u}_M, \mathbf{T}^{c}_M$ are:

$$[\mathbf{T}_M] = \begin{bmatrix} \sigma_1 & \tau \\ \tau & \sigma_2 \end{bmatrix}, \quad [\mathbf{T}^{u}_M] = \begin{bmatrix} \sigma^{u}_1 & \tau^{u} \\ \tau^{u} & \sigma^{u}_2 \end{bmatrix}, \quad [\mathbf{T}^{c}_M] = \begin{bmatrix} \sigma^{c}_1 & \tau^{c} \\ \tau^{c} & \sigma^{c}_2 \end{bmatrix}$$

and then Eq. (13) can be written into components as follows:

$$\begin{cases} \sigma_1 = (1-\beta)\sigma^{u}_1 + \beta\sigma^{c}_1, \\ \sigma_2 = (1-\beta)\sigma^{u}_2 + \beta\sigma^{c}_2, \\ \tau = (1-\beta)\tau^{u} + \beta\tau^{c}. \end{cases} \tag{14}$$

This means that the effective stress is expressed in each point as the weighted sum of an elastic "uncracked" contribution and a "cracked" one. The damage variable is actually the weighting factor for the local contributions to the overall stress state.

3.2.1. The microscopic constitutive laws

In this paragraph the constitutive behaviour of the two material fractions is described: the starting point is the elastic law expressed by (6) and (7), here adapted to take into account the presence of inelastic deformations. The given macro deformation is $\mathbf{E}_M$ and the microdeformation is governed by the localization choice implied by Voigt's procedure, that is $\mathbf{E}_M^{\mathrm{u}} = \mathbf{E}_M^{\mathrm{c}} = \mathbf{E}_M$. In the vector basis drawn in Fig. 6, the components of $\mathbf{E}_M$ are:

$$[\mathbf{E}_M] = \begin{bmatrix} \varepsilon_1 & \gamma \\ \gamma & \varepsilon_2 \end{bmatrix}.$$

3.2.1.1. "Uncracked" stresses. The behaviour of the uncracked fraction is linearly elastic in every step of the loading process, that is:

$$\mathbf{T}_M^{\mathrm{u}} = \mathbb{K}^E \mathbf{E}_M \rightarrow \begin{cases} \sigma_1^{\mathrm{u}} = St_{11}^E \varepsilon_1 + St_{12}^E \varepsilon_2, \\ \sigma_2^{\mathrm{u}} = St_{12}^E \varepsilon_1 + St_{22}^E \varepsilon_2, \\ \tau^{\mathrm{u}} = St_{33}^E \gamma \end{cases} \tag{15}$$

with the coefficients explicited in Eq. (7).

3.2.1.2. "Cracked" stresses. For the "cracked" fraction, we suppose that the constitutive behaviour depends on whether the crack is open or closed, that is, whether the macrostrain ε_2 is positive or negative. The microdeformation is always equal to the macrodeformation: the problem is to state which components are elastic and which are inelastic.

If the crack is closed, the material fraction behaves as it is intact and elastic (15); if appropriate, it will develop inelastic deformations in the shear direction, involving frictional phenomena. This means that the macroshear strain will be partly plastic (γ_{r}) and partly elastic ($\gamma - \gamma_{\mathrm{r}}$), according to Coulomb's frictional law. As pointed out in Section 2.2, γ_{r} represent the "memory" of the non-holonomic frictional time history.

$$\begin{cases} \sigma_1^{\mathrm{c}} = St_{11}^E \varepsilon_1 + St_{12}^E \varepsilon_2, \\ \sigma_2^{\mathrm{c}} = St_{12}^E \varepsilon_1 + St_{22}^E \varepsilon_2, \quad \textit{closed crack}. \\ \tau^{\mathrm{c}} = St_{33}^E (\gamma - \gamma_{\mathrm{r}}) \end{cases} \tag{16}$$

under the condition:

$$\Phi_S = \mid \tau^{\mathrm{c}} \mid + \mu \sigma_2^{\mathrm{c}} \leqslant 0 \tag{17}$$

If the crack is open, the idea is that ε_2 and γ are both anelastic and not involving plastic phenomena, while ε_1 is entirely elastic (see Fig. 9).

This elementary difference arises from simple considerations: even if open, the interface cracks are placed along direction 1 and divide the material in a set of parallel layers that allow the transmission of ε_1. Hence, according to the (7), τ^{c} is zero, σ_1^{c} is non-zero for the part depending on ε_1. Also σ_2^{c} would be non-zero for the part depending on ε_1, that is, $\sigma_2^{\mathrm{c}} = St_{12}^E \varepsilon_1^{\mathrm{c}}$. However, since Voigt's homogenization is based on displace-

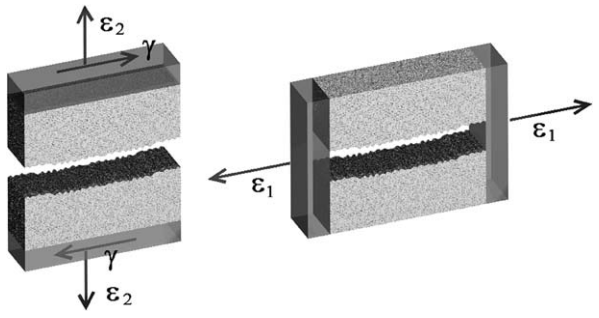

Fig. 9. The selective transmission of the elastic deformations for an open crack.

ments and implies approximation in stresses and equilibrium errors, $\sigma_2^c \neq 0$ should be considered as an equilibrium error (it does not satisfy a natural boundary condition on the open crack faces) and is therefore neglected.

Hence, for an open crack, the constitutive law is the following:

$$\begin{cases} \sigma_1^c = St_{11}^E \varepsilon_1 \\ \sigma_2^c = 0 \qquad \textit{open crack}. \\ \tau^c = 0 \end{cases} \tag{18}$$

3.3. The damage evolution law

It is now necessary to represent in an explicit form the cracks' evolution law as a function of the chosen damage variable β, according to the energetic criterion (4) sketched in Section 2.2:

$$\mathscr{G}[\mathbf{t}, \beta] - \mathscr{R}[\beta] \leqslant 0. \tag{19}$$

Until this condition is satisfied, β does not evolve and the cracks within the sampled joint do not propagate. The situation $\mathscr{G} = \mathscr{R}$ represents a critical condition and is to be considered as the starting point for the growth of the crack, proceeding by adjacent equilibrium states.

According to (3), the explicit computation of $\mathscr{G}$ involves the elastic strain energy expressed as a function of the damage variable through the inelastic contributions ε^* and γ^* (9), that will be now specified for the mortar material and for the new damage variable β. It should be clear that solution (2) has to be re-scaled in terms of this new variable and this implies a redefinition of the compliance parameters, to be experimentally tuned.

$$\begin{cases} \epsilon^* = \beta c_{\mathrm{mn}} \sigma_{2,\mathrm{eff}} = \beta c_{\mathrm{mn}} \mathscr{H}(\sigma_2)\sigma_2, \\ \boldsymbol{\gamma}^* = \beta c_{\mathrm{mt}} \tau_{\mathrm{eff}} = \beta c_{\mathrm{mt}}(\tau + f), \end{cases} \tag{20}$$

where, with the same notation used in Section 2.2:

c_{mn}, c_{mt} = normal and tangential compliance for the mortar;
$f = -\mathrm{sign}(\tau)\mathscr{H}(\sigma_2)\mu \mid \sigma_2 \mid$ = friction force.

By applying (3), the expression of the energy release rate $\mathscr{G}$ as a function of β becomes:

$$\mathscr{G} = \frac{1}{2}\frac{\mathrm{d}W_e}{\mathrm{d}\beta}\bigg|_{\sigma_2,\tau=\mathrm{cost}} = \frac{1}{2}\left[\mathscr{H}(\sigma_2)\sigma_2 \cdot \frac{\partial \epsilon_2^*}{\partial \beta} + (\tau + f)\cdot \frac{\partial \gamma^*}{\partial \beta}\right] = \frac{1}{2}\left[c_{\mathrm{mn}}\mathscr{H}(\sigma_2)\sigma_2^2 + c_{\mathrm{mt}}(\tau + f)^2\right]. \tag{21}$$

Let us now explicitly express the contributions of the cracked and uncracked fractions by introducing in (21) the homogenized Cauchy stress components (14):

$$\mathscr{G} = \frac{1}{2}\left\{c_{\mathrm{mn}}\mathscr{H}(\sigma_2)\left[(1-\beta)\sigma_2^u + \beta\sigma_2^c\right]^2 + c_{\mathrm{mt}}\left[(1-\beta)(\tau+f)^u + \beta(\tau+f)^c\right]^2\right\}.$$

Under tension ($\varepsilon_2 \geqslant 0$), the average operator provides that all the stress components of the cracked fraction actually appearing in $\mathscr{G}$ vanish. Hence, we will have:

$$\mathscr{G}^+ = \frac{1}{2}(1-\beta)^2\left\{c_{\mathrm{mn}}\sigma_2^{u2} + c_{\mathrm{mt}}\tau^{u2}\right\} \quad \textit{open crack}\ (\varepsilon_2 \geqslant 0).$$

Under compression ($\varepsilon_2 < 0$), the expression of the energy release rate $\mathscr{G}$ deserves more attention. First of all, $\mathscr{G}$ does not include the contribution of the compressive normal stress, because in our damage model compressive stress does not spend work for opening the cracks. The tangential stress has to be slightly manipulated in order to show the role played by Voigt's homogenization:

$$\begin{aligned} \tau &= \beta\tau^c + (1-\beta)\tau^u = \beta\mu\sigma_2^c + (1-\beta)\tau^u = \beta\mu\sigma_2^c + (1-\beta)\mu\sigma_2^u - (1-\beta)\mu\sigma_2^u + (1-\beta)\tau^u \\ &= \mu\sigma_2 + (1-\beta)(\tau - \mu\sigma_2)^u \ \rightarrow\ \tau - \mu\sigma_2 = (1-\beta)(\tau - \mu\sigma_2)^u, \end{aligned}$$

so, we will have:

$$\mathscr{G}^{-} = \frac{1}{2}(1-\beta)^2 c_{\mathrm{mt}}(\tau + f)^{\mathrm{u}2} \quad \textit{closed crack } (\varepsilon_2 < 0).$$

In a concise form, we can express the two previous equations in the following formula:

$$\boxed{\mathscr{G} = \tfrac{1}{2}(1-\beta)^2 \left\{ c_{\mathrm{mn}} \mathscr{H}(\sigma_2)\sigma_2^{\mathrm{u}2} + c_{\mathrm{mt}}(\tau + f)^{\mathrm{u}2} \right\}}. \tag{22}$$

Still it has to be explicited the expression for $\mathscr{R}$, which will contain the mechanical response of the material with respect to fracture. The equation of $\mathscr{R}[\beta]$ is chosen on a semi-empirical base, following the classical guidelines for concrete-like materials, which can be found in the literature (Broek, 1984). The chosen $\mathscr{R}$-function represents the essential behaviour of a quasi-brittle material, which typically includes an initial stable branch and an unstable softening phase, separated by a critical state $(\beta_{\mathrm{cr}}, \mathscr{R}_{\mathrm{cr}})$ which is experimentally identified:

$$\mathscr{R}[\beta] = \begin{cases} R_{\mathrm{mcr}} \dfrac{\beta}{1-\beta} & 0 \leqslant \beta \leqslant \beta_{\mathrm{cr}}, \\ R_{\mathrm{mcr}} \left\{ \dfrac{\beta}{1-\beta} \right\}^{-\rho_{\mathrm{m}}} & \beta_{\mathrm{cr}} \leqslant \beta \leqslant 1, \end{cases} \tag{23}$$

$$\rho_{\mathrm{m}} = 0.8. \tag{24}$$

The plot of this function is shown in Fig. 10. The maximum of the function is:

$$R_{\mathrm{mcr}} = c_{\mathrm{mn}} \sigma_{\mathrm{lim}}^2 = c_{\mathrm{mt}} \tau_{\mathrm{lim}}^2 \tag{25}$$

and is attained for $\beta = \beta_{\mathrm{cr}} = 1/2$.

Now, the relation $\mathscr{G}(\beta) - \mathscr{R}(\beta) = 0$ allows to associate at each value of the total strain $\mathbf{E}$ the damaged state β of the material point under investigation. A few manipulations of (22) and (23) lead to the following equations, the first of which is valid in the stable branch $0 \leqslant \beta \leqslant 1/2$, the second in the unstable one $1/2 \leqslant \beta \leqslant 1$:

$$\begin{cases} y = R_{\mathrm{mcr}} \dfrac{\beta}{(1-\beta)^3} & 0 \leqslant \beta \leqslant \dfrac{1}{2}, \\ y = R_{\mathrm{mcr}} \dfrac{1}{\beta^{\rho_{\mathrm{m}}}(1-\beta)^{2-\rho_{\mathrm{m}}}} & \dfrac{1}{2} \leqslant \beta \leqslant 1, \end{cases} \tag{26}$$

where it has been set $y = \frac{1}{2}\left[c_{\mathrm{mn}}\sigma_2^{\mathrm{u}2} + c_{\mathrm{mt}}\tau^{\mathrm{u}2}\right]$.

The two functions have been plotted in Fig. 11 in the whole domain $0 < \beta < 1$: however, the branches of our interest are only those drawn by continuous line.

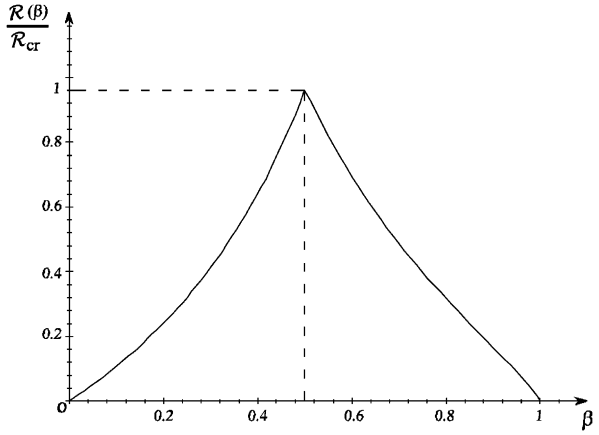

Fig. 10. Toughness function $\mathscr{R}(\beta)$.

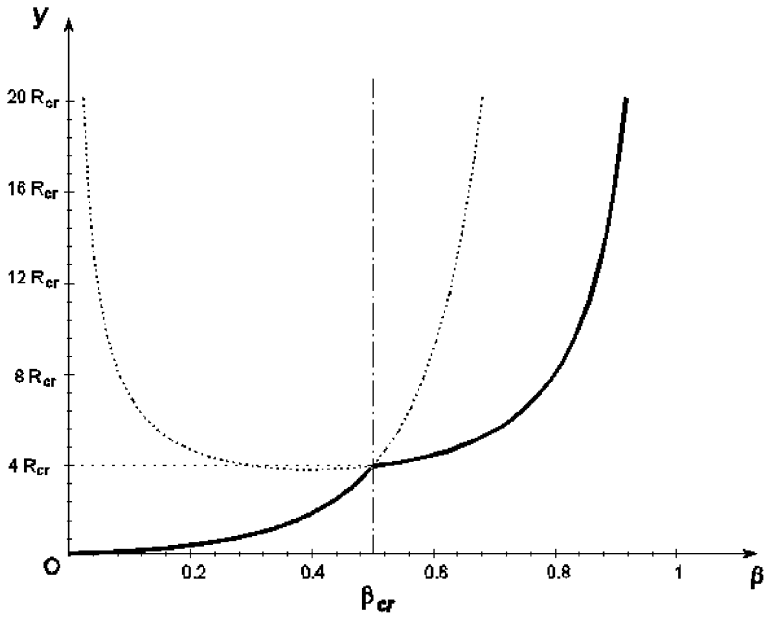

Fig. 11. Plot of the diagram β–y.

Eq. $(26)_1$ can be easily inverted, obtaining an explicit expression for β. Function $(26)_2$, instead, does not admit an analytic inverse function and, from an algorithmic point of view, it is convenient to perform a piecewise linearization. Another algorithmic drawback is the presence of the cusp for $\beta = 0.5$, which can be conveniently smoothed.

We have used an elastoplastic constitutive model with damage. In order to calibrate the macroscopical model, a set of micromechanical parameters, both elastic and inelastic, have to be identified.

Roughly speaking, in the literature there are two different classes of experimental tests aimed at the identification of the micromechanical parameters of masonry. A first category directly involves the individual constituents of the masonry (i.e. mortar and bricks), and includes standard tests for the determination of their elastic coefficients (the constituents are supposed to have an isotropic, elastic behaviour).

A second class of tests, instead, is aimed at the specific characterization of the "mortar joint" (intended as the assembly of mortar beds and bricks), which is deeply governed by the presence of interface layers.

In the literature about the constitutive modelling of masonry, a frequent choice is to introduce the micromechanical parameters belonging to the first group into a linear homogenization procedure, in order to obtain the elastic properties of the composite material at the macroscopic level. For the description of the inelastic behaviour of the mortar joint, a wide variety of constitutive models can be used. Anyway, recurrent parameters are: the ultimate strength of the joint under tension and shear, the friction coefficient, the dilatancy. These parameters are measured from specific tests on small combinations of bricks and mortar (couplets and triplets).

In our model, mortar joints are very thin if compared to the bricks' height and it is quite intuitive to consider as crucial the role of the mortar–brick interfaces. Therefore, we have chosen to use the constitutive parameters provided by the tests on couplets and triplets rather then those measured on mortar specimens.

More specifically, the damage law we have used (19) involves four different mechanical parameters: the ultimate strength under tension (σ_{lim}); the ultimate strength under shear (τ_{lim}); the axial compliance of the mortar joint (c_{mn}); the tangential compliance of the mortar joint (c_{mt}). Actually, only three of these coefficients can be independently assigned (see Eq. (25)). Hence, according to the specific test to be simulated, the axial or the tangential compliance of the joint is deduced from the experimental tests, while the other one is numerically defined by Eq. (25): $R_{\text{mcr}} = c_{\text{mn}}\sigma_{\text{lim}}^2 = c_{\text{mt}}\tau_{\text{lim}}^2$.

The development of damage and frictional sliding are, at this point, uncoupled: the former is directly determined from the total strain assigned at the beginning of the load step; the latter only involves the cracked

portion of the material, whose amount is measured by the actual value of β (which can be immediately calculated, according to the previous remark). Since the frictional law is non-holonomic, the inelastic residual sliding γ_r must be known throughout all the loading process. In order to do this, we will store at each step the difference between the uncracked tangential stress and the cracked one, that is an information perfectly equivalent to the accumulated residual sliding, as shown in Fig. 16.

3.4. FEM numerical analysis

3.4.1. Integration strategy

The mechanical behaviour of the masonry material described in the last sections is now inserted within a FEM integration strategy, driven by a scalar loading parameter λ. The equilibrium equations of the discretized problem:

$$\mathbf{s}[\mathbf{u}] - \mathbf{p}[\lambda] = \mathbf{0},$$

where $(\mathbf{s}, \mathbf{u}, \mathbf{p}) \in \mathscr{R}^n$ and $\lambda \in \mathscr{R}$, are highly non-linear and actually governed by the constitutive behaviour of the mortar joints.

The solution algorithm chosen is a step-by-step evolutive one, consisting in a linear elastic prediction followed by an iterative correction phase (see Fig. 12), based on Modified Newton Raphson strategy. The control parameter is the arc-length, which is able to avoid the loss of convergence at the limit load configurations (Riks, 1979, 1984).

In Fig. 13 the flow chart of a single step of the arc-length iterative algorithm is pictured.

Starting from the two last known equilibrium configurations (0 and 1 in *initial point*), a linear extrapolation is performed (*predictor*) driven by a parameter ω which takes into account the non-linear behaviour of the previous steps. Then, starting from a first trial configuration $\tilde{2}$, an iterative correction phase begins, aimed at zeroing the equilibrium residual. Such a phase consists in the calculation of the elasto-plastic response ($\mathbf{s}[\mathbf{u}_j]$ in *structural response*), of the residual vector ($\mathbf{r}_j$ in *equilibrium residual*), of the primary variable correction vectors ($\dot{\mathbf{u}}_j, \dot{\lambda}_j$ in *corrector*), and finally in the updating step ($\mathbf{u}_{j+1}$, λ_{j+1} in *updating*). At each iteration of the correction phase, the constitutive information of each mortar joint is updated. This is done in the routine called "elastoplastic structural response", discussed in Section 3.4.3, where the global stress state, the current values of the internal variables and the structural response at four Gauss integration points for each element are calculated (Fig. 7).

3.4.2. High-continuity FEM discretization

With regard to the FEM discretization, the algorithm handles a mesh of rectangular compatible finite elements, for which a High Continuity interpolation (see Aristodemo, 1985) is chosen. Each finite element has a single node, located at the center of the element itself, with two parameters. However, the displacement fields

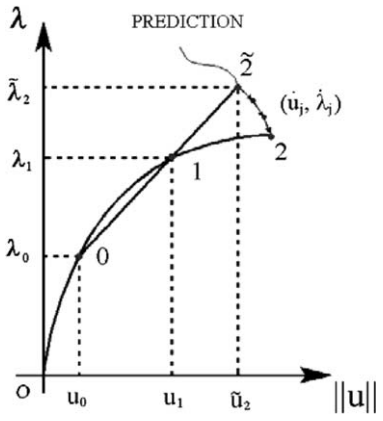

Fig. 12. The reconstruction of the equilibrium path: step-by-step evolutive analysis and arc-length iterative strategy.

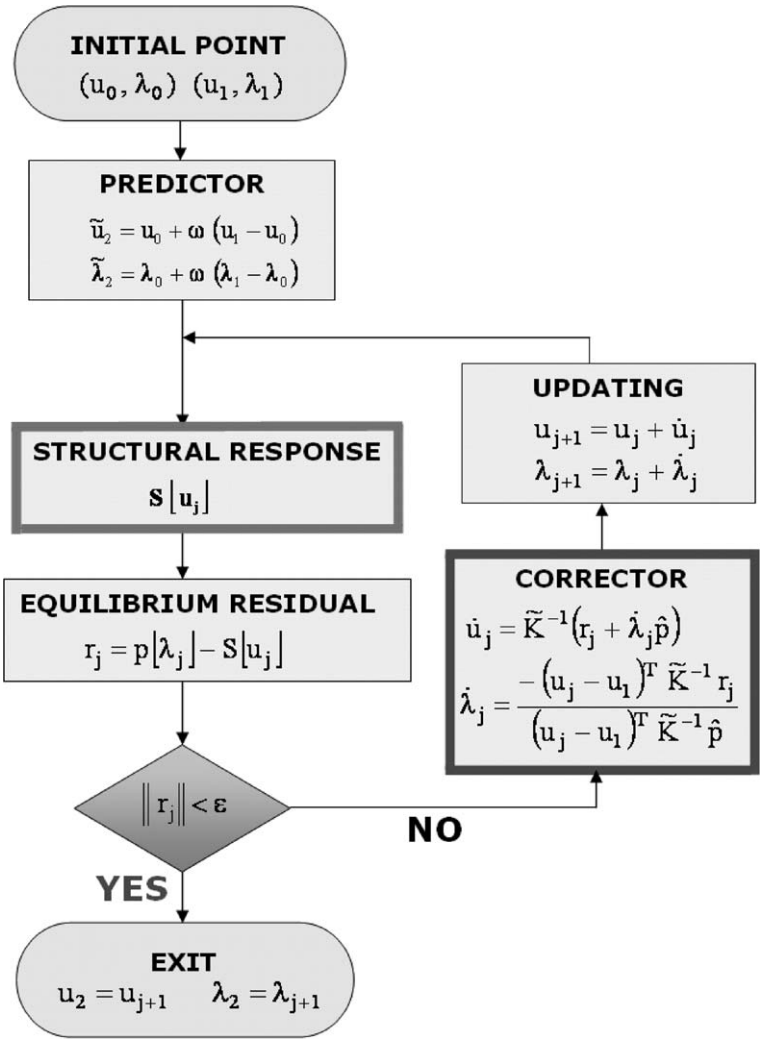

Fig. 13. Flow chart of the integration strategy.

of the element are interpolated by quadratic splines, by using all the parameters of the eight surrounding elements. This guarantees a C^1-continuity to the displacements and a C^0-continuity to the deformations, even if a relatively small number of parameters is used, and enables the use of the element in computational elastoplastic problems. Moreover, the regularity of a rectangular mesh is fairly suitable for the analysis of masonry panels with a standard geometry.

Let us now refer to Fig. 14 in order to present further details of the finite element in the case of a two-dimensional problem. Each internal finite element is surrounded by a grid of eight elements, from which it gains the parameters needed for the interpolation of the displacement fields in its domain. For example, in the grid of nine elements shown in Fig. 15(a) numbered like the entries of a 3×3 numerical matrix, the element 2,2 uses nine nodal parameters d_{ij}, $i,j := 1,3$ (one for each element) for each displacement fields. For example, the variation law of $u(\xi,\eta)$, expressed in terms of the natural coordinates $\xi = \frac{x}{a}$ and $\eta = \frac{y}{b}$ (where a and b are respectively the width and the height of the element), of the nodal parameters d_{ij} and of the shape functions Φ_i, assumes the following form:

$$u(\xi,\eta) = \sum_{i,j=1}^{3} \Phi_i(\xi)\Phi_j(\eta)u_{ij},$$

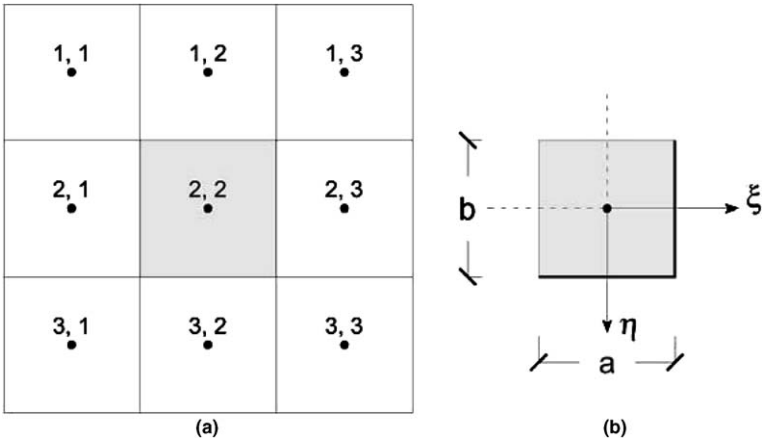

Fig. 14. (a) Nodes' position for a standard HC grid; (b) Natural coordinates.

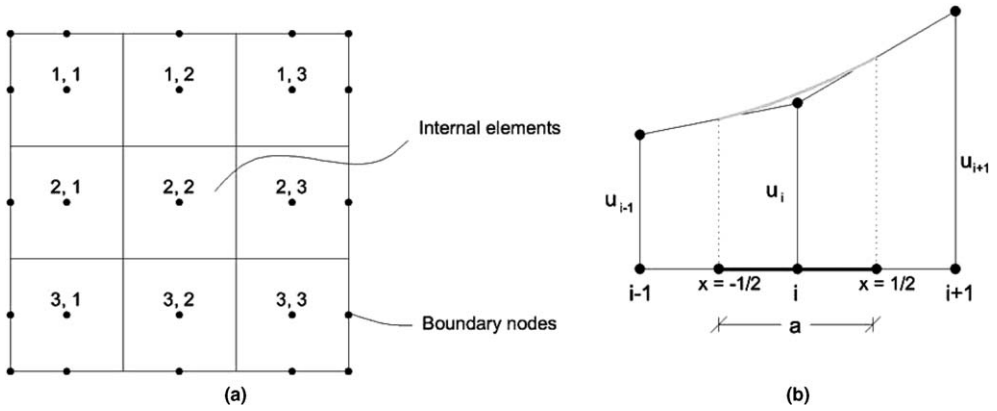

Fig. 15. (a) Nodes' position for the FE at the boundary; (b) Displacement interpolation for the one-dimensional case.

where the Φ_i, obtained by imposing the continuity condition on u and on its derivatives along directions x and y, are:

$$\Phi_1(\xi) = \frac{1}{8} - \frac{\xi}{2} + \frac{\xi^2}{2} \quad \Phi_1(\eta) = \frac{1}{8} - \frac{\eta}{2} + \frac{\eta^2}{2},$$

$$\Phi_2(\xi) = \frac{3}{4} - \xi^2 \qquad \Phi_2(\eta) = \frac{3}{4} - \eta^2,$$

$$\Phi_3(\xi) = \frac{1}{8} + \frac{\xi}{2} + \frac{\xi^2}{2} \quad \Phi_3(\eta) = \frac{1}{8} + \frac{\eta}{2} + \frac{\eta^2}{2}.$$

This "cellular" structure, although privileged among the compatible elements of the same computational cost, implies some drawbacks. In fact, the overall management becomes somewhat cumbersome because of the elements at the boundary. These are special elements, since they lack some of the nodes that are needed in the interpolation. Therefore, just for the elements at the boundary, further nodes are introduced along the boundary itself (see Fig. 15(a)), and there is a specialized treatment with respect to the standard elements. In particular, depending on which part of the boundary they do share, the shape functions assume specific definitions (see Aristodemo, 1985).

3.4.3. The elastoplastic structural response algorithm

With reference to Fig. (13), it will be now better precised how the structural response is constructed at each iteration of the correction phase:

1. A first trial displacement field **u** is assigned and the correspondent compatible deformation field $\mathbf{E}_M$ is defined. Starting from this, it is immediately computed the local stress state $\mathbf{T}_M$, split into two fractions (''uncracked''–''cracked''): $\mathbf{T}_M^u, \mathbf{T}_M^c$. In this phase, also the increment of the internal damage variable β is evaluated, by using (26).

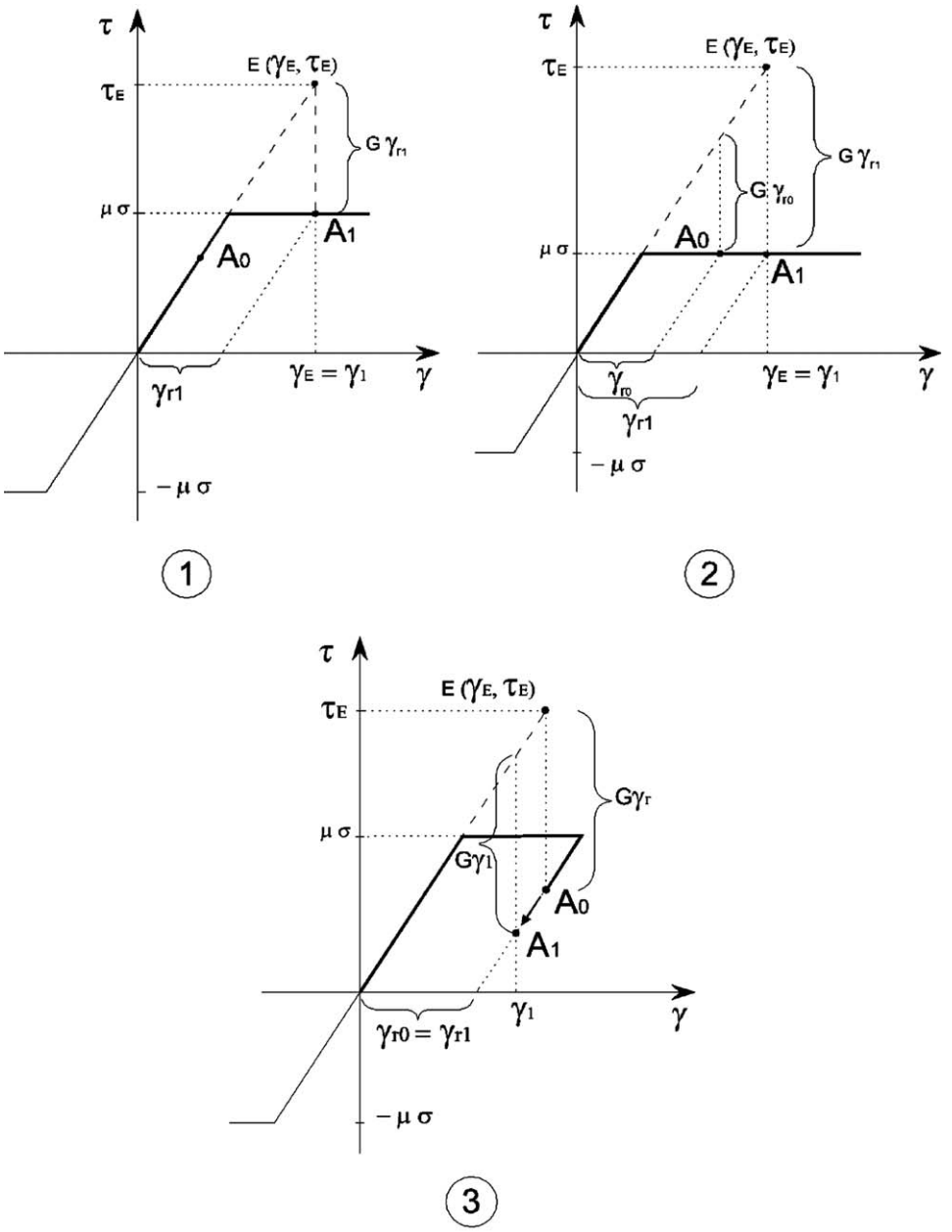

$\mathbf{A_0}$ = initial state; $\mathbf{A_1}$ = final state; $\mathbf{E}$ = elastic prediction

Fig. 16. Frictional model and residual sliding.

2. At this point, it is faced the truly plastic part of the constitutive law: the elastic stress prediction, when violating the plastic admissibility condition, is corrected in order to bring back the actual elasto-plastic stress state within the limit domain (according to a typical return algorithm). As previously specified, only the cracked portion of the material (singled out by β) is involved, and moreover the nature of the plastic deformations is purely tangential. The plastic condition to be checked is represented by Eq. (17), that identifies the classical Mohr–Coulomb cone. According to the classical framework of the Theory of Plasticity, elastic and inelastic strain contributions are supposed to follow an additive law (where the plastic variable governing the evolution of the limit domain is the accumulated plastic sliding γ_r):

$$\gamma_{EP} = \gamma_E + \gamma_r. \tag{27}$$

So, when the plastic condition (17) is activated, the final admissible stress state is recovered and the plastic variable γ_r is updated by (27).

$$\text{Calculation of the final state: } \begin{cases} \gamma_1 = \gamma_E, \\ \tau_1 = \max(-\mu\sigma, \min(\tau_E - G\gamma_{ro}, \mu\sigma)), \end{cases}$$

$$\text{Updating of the residual sliding: } \gamma_{r1} = (\tau_E - \tau_1)/G.$$

If we plot the elastoplastic law in the τ–γ plan, a geometrical interpretation tells us that the elastic prediction point (**E**) and the elastoplastic solution (**A**1) are on the same vertical line, that is to say, correspond to the same total tangential sliding γ. In Fig. 16, this graphical interpretation of the inelastic tangential sliding and of the final elastoplastic state is shown, with regard to three different initial states.

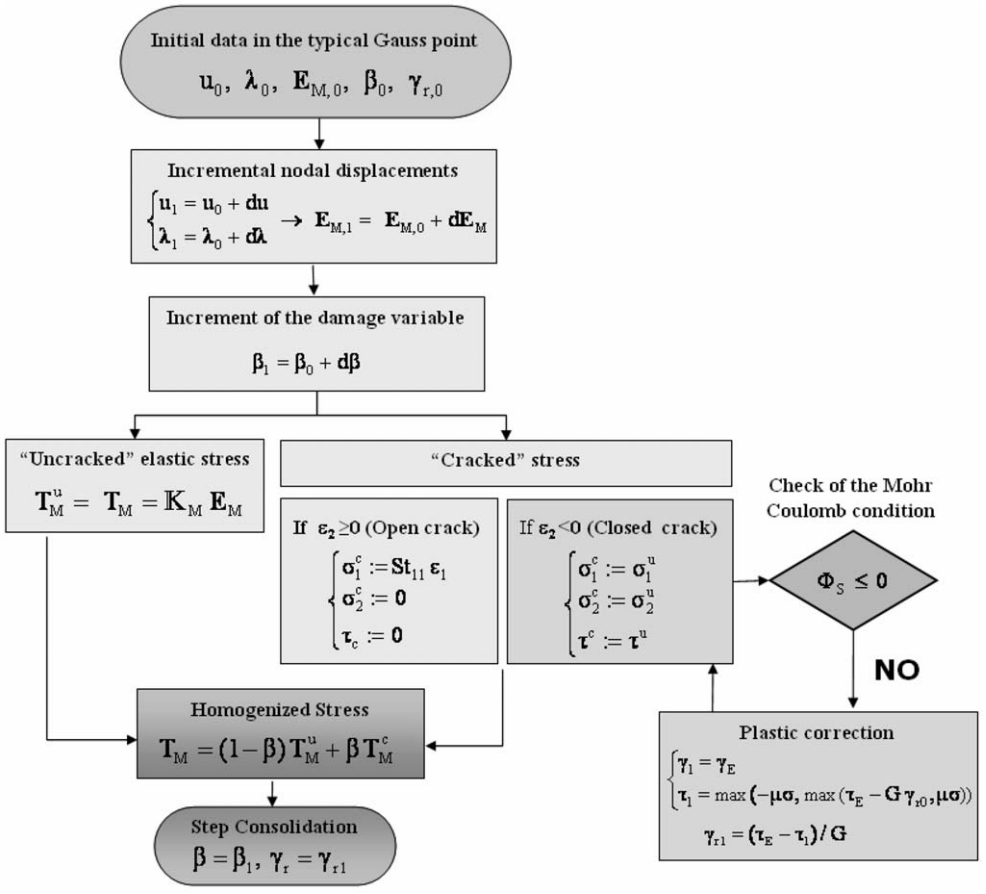

Fig. 17. Flow chart showing the computation of the elastoplastic structural response.

3. The "*homogenized*" stress is recovered by adding up the uncracked and the cracked contributions, properly weighted by the actual value of β (Eqs. (13) and (14)).

The routine for the calculation of the elastoplastic structural response, as it is implemented in the numerical code is summarized in the flow chart of Fig. 17.

4. Numerical tests: results and discussion

The computational model previously described allows a quite simple mechanical description of the examined phenomena. First of all, this has made the FE numerical implementation simple, and has provided a tool for explaining some characteristic phenomenological evidences, assessing a set of benchmarks and preliminary tests, in view of the future tuning of both the mechanical and the computational model.

In the following paragraphs, a number of simple tests are presented, in order to show how the behaviour under simple tension, compression and shear is reproduced for small representative elements. Then, two experimental tests for masonry brick specimens have been chosen to be numerically reproduced. The scope was to investigate the potentiality and accuracy of the followed approach, making also clear the limits and problems to be furtherly faced. Results are encouraging enough, showing a satisfactory reconstruction of the main features of the structural behaviour, with a fairly cheap computational cost.

4.1. Basic benchmarks: cyclical tensile and shear tests for small panels

As first reference examples, in order to assess the basic performances of the code, simple tests (cyclical uniaxial tension and cyclical shear under constant compression) for a small structural element are presented (the mechanical parameters used are the same listed in Table 2). In Fig. 18, the masonry geometric pattern, loading and constraint schemes are drawn, together with the chosen mesh (4 HC elements). The left bottom element is enlightened in order to make clear that the computational model is different from the initial geometric scheme because of the neglection of head joints. The symbol λ identities the varying load. At the bottom of the same figure, stress–strain diagrams in a specific Gauss-point (the one marked in bold) are drawn. As expected, in the cyclical shear test the presence of hysteresis loops is observed: at the beginning, sliding is inhibited by the friction force, and the unloading follows the line tangent to the curve at the origin (the apparent tangential modulus is the same than the initial structure); when the applied stress exceeds the friction force, a sliding takes place, and there is a sudden change in the slope of the line. As a consequence, a permanent tangential deformation arises, and a part of the elastic energy is dissipated.

4.2. Monotonic shear test on a masonry panel

A larger numerical test has been performed on a test proposed by Raijmakers and Vermeltfoort in Raijmakers and Vermeltfoort (1992), in which a masonry periodic brickwork has been experimentally tested under a monotonic load.

The pier is a one-wythe running bond masonry, built using 20.4 cm × 9.8 cm × 5.0 cm clay blocks and mortar joints of thickness $s = 1.0$ cm, according to the arrangement shown in Fig. 19. The overall dimensions of the pier are: $B = 100$ cm, $H = 100$ cm, $T = 100$ cm, and the loading set-up and pattern are schematized in Fig. 19.

The numerical simulation of this test has been performed with our algorithm, by using a mesh of 40 HC elements and 66 nodes. The geometrical scheme and the mesh are shown in Fig. 20.

It is worth noting that, in order to fit the actual dimensions of the specimen with the reference cell adapted to the specific brick pattern (see Fig. 7, bottom), a small variation in the geometry has been adopted ($B = 108$ cm, $H = 98$ cm). In the report describing the benchmarks (Raijmakers and Vermeltfoort, 1992), the uniaxial tests on mortar, bricks and masonry specimens are also presented. As pointed out in Section 3.3, the mechanical parameters used in the algorithm proposed by the authors are just identified by means of these simple reference values. The mentioned data have been provided in the reference: the corresponding

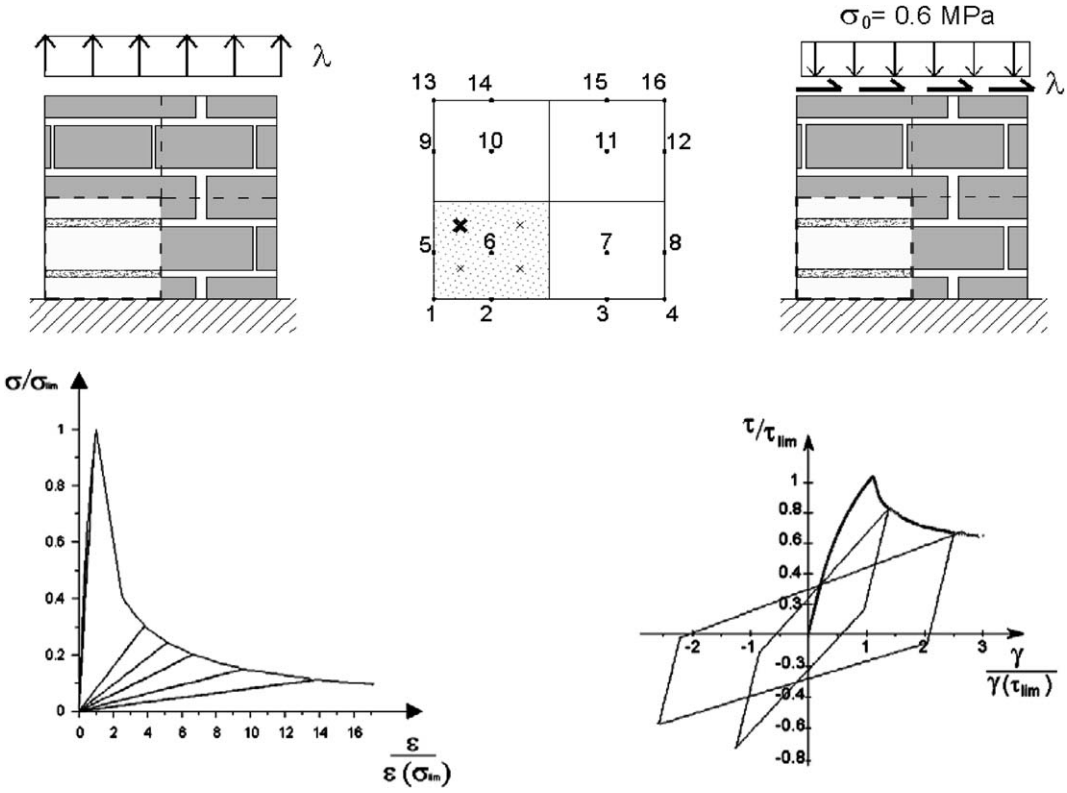

Fig. 18. Basic benchmark tests for tension (left) and shear (right): schemes of the masonry elements, mesh and stress–strain diagrams for the Gauss-point marked in bold.

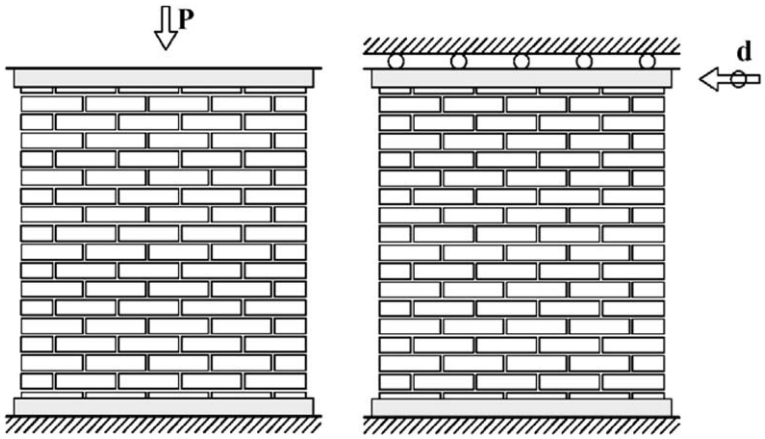

Fig. 19. Geometry and loads of the experimental test of Raijmakers and Vermeltfoort (1992): vertical load (left) and horizontal quasi-static load (right).

coefficients, according to the identification scheme indicated in Section 3.3, and used in our model, are listed in Table 1.

It is worth making some comments on the results of the numerical analysis, shown in the next three figures. Fig. 21 presents a comparison among two experimental curves (one for each specimen shown in Fig. 22), the equilibrium curve provided by our algorithm and the numerical curve provided by Lourenço et al. in

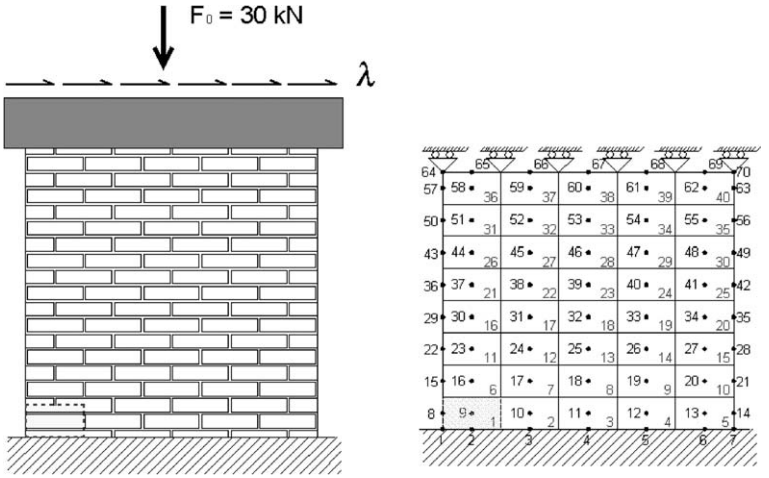

Fig. 20. Numerical simulation of the test of Raijmakers and Vermeltfoort (1992): geometrical scheme and FE mesh.

Table 1
Mechanical parameters of the constituents

Mortar	Bricks
$E_m = 780$ MPa	$E_b = 16{,}700$ MPa
$\nu_m = 0.125$	$\nu_b = 0.15$
$\sigma_{lim} = 0.25$ MPa	
$\tau_{lim} = 0.35$ MPa	
$\mu = 0.75$	
$\eta_m = 0.167$	
$c_{mn} = 0.0154$ MPa^{-1}	
$\rho_m = 0.8$	

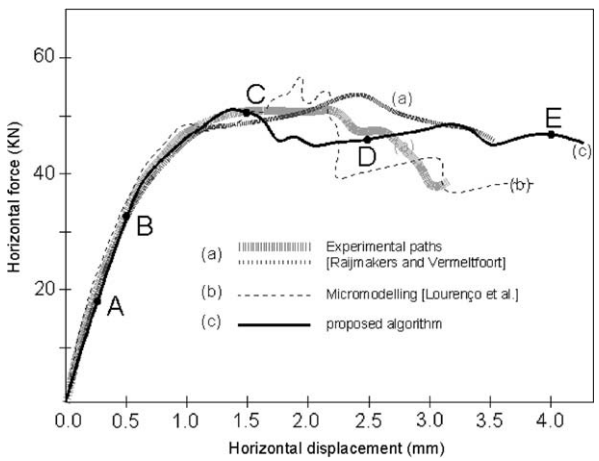

Fig. 21. Comparison among the experimental curves, the results provided by our algorithm and the results of Lourenço et al.

Lourenço et al. (1994) by a discrete approach, based on 648 finite elements. The simulation based on our model showed some numerical swaying in the reconstruction of the post-critical branch of the equilibrium curve; nevertheless, a satisfactory matching with the experimental results of Raijmakers and Vermeltfoort

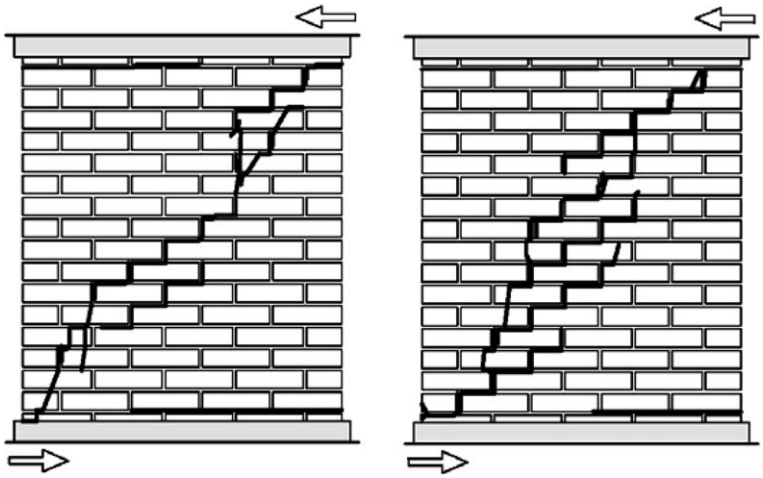

Fig. 22. The experimental crack pattern for two of the specimens.

and the numerical results of Lourenço et al. has been obtained, also considering that the recorded numerical drifting is comparable to the scattering of the available experimental results.

In Fig. 23 the progressive development of the damage (as reproduced by our algorithm and represented by the value of the damage variable β) is shown in correspondence of the five points A, B, C, D, E of the equilibrium curve. In Fig. 22, the qualitative experimental failure patterns are drawn, and they can be compared with the numerical damage maps. It should be clear that our algorithm in unable of reproducing the brick crushing and the development of cracks within head joints. However, the progressive diagonal crack patterns and the progressive horizontal sliding patterns of the first and the last rows are well reproduced.

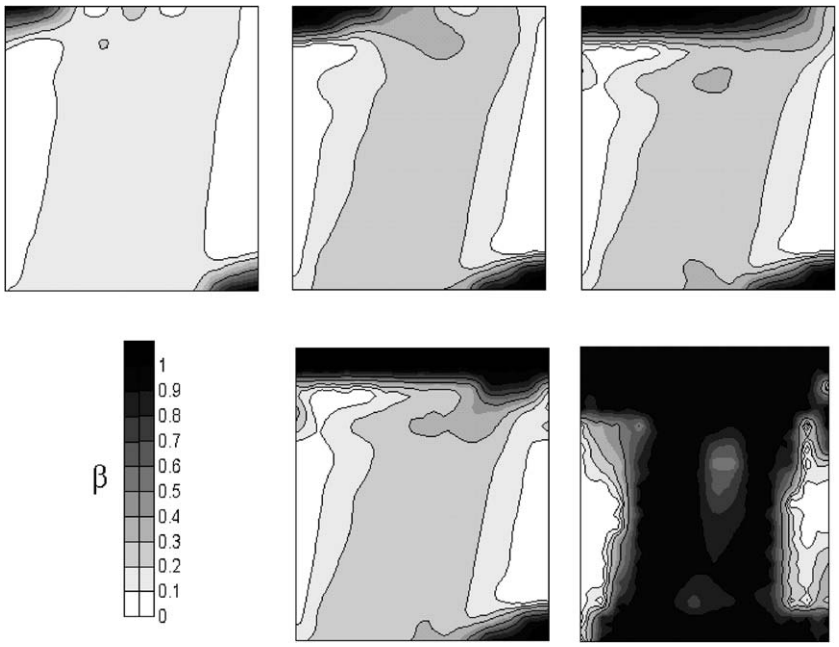

Fig. 23. Damage distribution at points A–E of Fig. 21.

4.3. Cyclical shear test on a masonry panel

The results presented in this subsection are relative to a famous benchmark due to Anthoine et al. (1994) and performed at ISPRA. The geometry of the analyzed panel is shown in Fig. 24, together with the test set-up and load pattern. After applying a constant vertical preload, the panel has been subjected to a cyclical shear loading. The results provided by our algorithm have been compared not only with the experimental ones but also with the numerical results obtained by Gambarotta et al. (1995) through the micromechanical model described in Gambarotta and Lagomarsino (1994a), Gambarotta (1995), Gambarotta and Lagomarsino (1993, 1994b).

The numerical simulation of the benchmark has been performed with our algorithm, by using a mesh of 70 HC elements and 104 nodes. The geometrical scheme and the mesh are shown in Fig. 25.

The parameters for the materials constituting the brickwork are listed in Table 2 (the volume fraction of the mortar is $\rho_m = 0.154$).

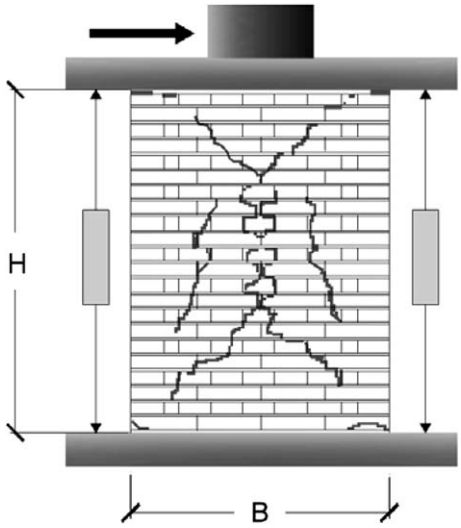

Fig. 24. Schematic testing set-up and crack pattern of the experimental test of Anthoine et al.

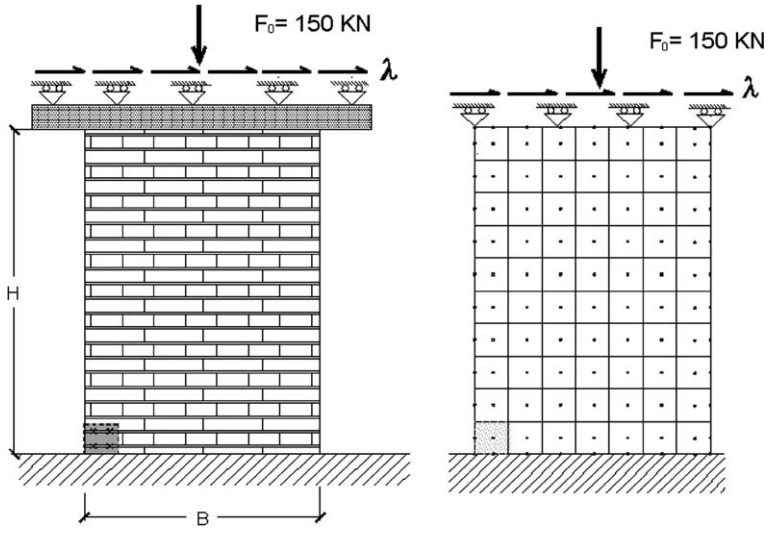

Fig. 25. Numerical simulation of the test with the proposed algorithm: schemes of the panel and FE mesh.

Table 2
Mechanical parameters (Anthoine et al., 1994)

Mortar	Bricks
$E_m = 650$ MPa	$E_b = 3000$ N/mm^2
$\nu_m = 0.15$	$\nu_b = 0.25$
$\sigma_{l,m} = 0.1$ MPa	$\sigma_{lb} = 5$ N/mm^2
$\tau_{l,m} = 0.25$ MPa	$\tau_{lb} = 2$ N/mm^2
$c_{mn} = 0.0154$ MPa^{-1}	$c_{bt} = 0.5$ MPa^{-1}
$\rho_m = 0.16$	$\rho_b = 0.16$
$\beta_m = 0.8$	$\beta_b = 0.9$

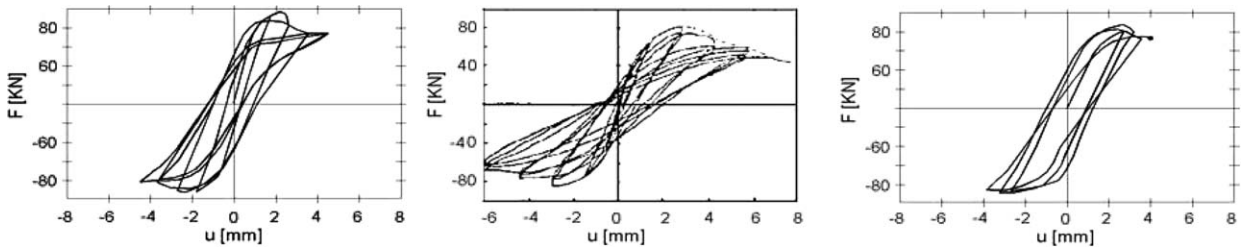

Fig. 26. Comparison of the results obtained with our algorithm (right), experimental tests (center) and Gambarotta's algorithm (left).

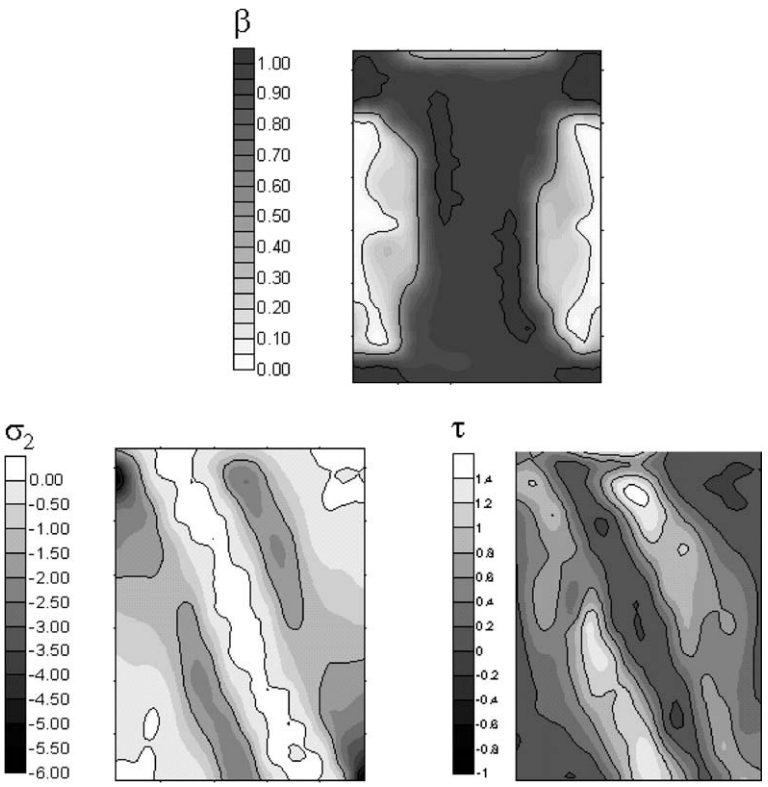

Fig. 27. Normal stress and damage distribution.

A first comparison among the results provided by our algorithm, the experimental results and Gambarotta's numerical results can be made in terms of equilibrium paths, as shown in Fig. 26. It is immediately clear that there is a significant difference between the numerical simulations and the experimental results: in fact the

latter involve a larger number of cycles and longer post-critical branch. Therefore, the comparison is necessarily partial. However, by the observation of the figure it can be deduced that both the numerical algorithms reproduce the limit configuration with a sufficient accuracy, even if with a slight overestimation of the limit load, probably because of the compatibility of both FE discretizations. In our algorithm, moreover, it should be noticed that the infinite strength of the bricks can be a further cause of the overestimation of the limit load, whereas the inability in following the hysteresis cycles in the advanced post-critical branch could depend on the numerical instability produced by the integration of the damage law.

A final comment has to be made about the crack patterns exhibited by the experimental test and those provided by the proposed model. In Fig. 27 the damage map and the stress state for the last equilibrium configuration obtained are reported. The damage map can be compared with the failure mechanism depicted in Fig. 24, which shows a crossed diagonal cracking due to the inversion of the load sign, plus a sliding shear cracking concentrated at the four corners of the panel. Within the capabilities of our model, whose limits have already been discussed, the figure demonstrate a fair good agreement with the experimental evidence.

5. Conclusions

The analysis we have performed has produced results quite satisfactory, and represents a starting point to be furtherly improved, under the key idea that both the model and the algorithm for the integration of the solution equations should be developed.

In the presented analysis, we have proposed three different levels, which are hierarchically interconnected one with the other: to each level a specific mathematical model corresponds, even if it is not always explicitly formulated. The three models are: the macroscopic model, which sees a Cauchy homogeneous continuum crossed by planes on which inelastic deformations develop; the mesoscopic level, in which the contributions of the mortars and the blocks can be clearly distinguished; the microscopic model, inside the cracked joint, where the dissipative phenomena (that are recorded in terms of stress state and internal damage and plastic sliding variables) occur. Of course, in each these levels, a well-founded mechanically improvement could be introduced.

With regard to the macroscopic level, the choice of a Cauchy continuum is maybe not the best possible, above all in a long perspective. In fact, if until now we have worked with a fixed mesh, using a Gauss sampling point at each mortar joint, varying the mesh size we would probably encounter mesh-dependence phenomena, that are well known in the literature (de Borst, 1991) and invariably affect a FEM analysis every time that a softening constitutive behaviour in introduced.

This is the first aspect that has to be improved in order to make the model more reliable and effective at the same time. Some steps forward in this direction have already be taken, by introducing at the macroscopic level a Cosserat Model (see Masiani et al., 1995; Salerno and Uva, 2002).

At the mesoscopic level, while neglecting head joints (that has been made for the sake of the mechanical and algorithmic simplicity) we have actually ignored the influence of the masonry texture on the solution. In the case of shear tests, the presence of head joints makes the real difference, for example, between a running bond masonry and a stack bond one (see di Carlo, 1999; Berto et al., 2004). This is an aspect to be improved, as well.

At the microscopic level, our idea is that the main part of the phenomenology involved has been taken into account (that is to say, the two crucial phenomena of damage and friction). Anyway, a deeper comprehension of the micromechanics could lead to a better-founded damage evolution law and, above all, to a smoother formulation, able to avoid the difficulties actually encountered in the integration of the law. With regard to this last aspect, a necessary improvement concerns the management of internal variables as primary variables of the problem (at the same level as displacement variables), as shown in Formica et al. (2003). This would allow, in our opinion, a fair good improvement in the stability of the algorithm.

Besides the enrichment of the model at the different levels, our primary forthcoming objective is to make the multiscale strategy more clear, expliciting the operators for the scale switching. Homogenization theory represents in this sense a very well assessed framework, able to suggest wise choices and carefully control the approximations and errors involved in every down or up-scaling that is performed (see Salerno and de Felice, 2000). It is indeed this aspect that has driven us in the choice of the paper title, with the purpose of pointing out that we really feel ourselves on a long road.

References

Alpa, G., Gambarotta, L., 1990. Mechanical models for frictional materials. In: Proc. of International Meeting on New Developments in Structural Mechanics, Catania.

Anthoine, A., 1994. Research on unreinforced masonry at the joint research center of the European commission. In: Proc. of the US Italy Workshop on Guidelines for Seismic Evaluation and Rehabilitation of Unreinforced Masonry, Pavia, pp. 427–432.

Anthoine, A., Magenes, G., Magonette, G., 1994. Shear compression testing and analysis of brick masonry walls. In: Proc. of 10th European Conference on Earthquake Engineering, Vienna, pp. 1657–1662.

Aristodemo, M., 1985. A high continuity finite element model for two-dimensional elastic problems. Comput. Struct. 21 (5), 987–993.

Asteris, P.G., 2003. Lateral stiffness of brick masonry infilled plane frames. J. Struct. Eng.: Amer. Soc. Civil Eng. (ASCE) 129.

Asteris, P.G., Tzamtzis, A.D., 2003. On the use of a regular yield surface for the analysis of unreinforced masonry walls. Electron. J. Struct. Eng. 3, 23–42.

Ballio, G., Calvi, G.M., Magenes, G., 1993. Experimental and numerical research on a brick masonry building prototype. Report 2.0, CNR-GNDT, Dipartimento di Meccanica Strutturale del'Universitá di Pavia.

Berto, L., Saetta, A., Scotta, R., Vitaliani, R., 2004. Shear of masonry panel in parametric FE analyses. Int. J. Solids Struct. 41, 4383–4405.

Broek, D., 1984. Elementary Engineering Fracture Mechanics, third ed. Martinus Nijhoff Publishers, The Hague, The Netherlands.

Budiansky, B., O'Connell, J., 1976. Elastic moduli of a cracked solid. Int. J. Solids Struct. 15, 81–97.

de Borst, R., 1991. Simulation of strain localization: a reappraisal of the cosserat continuum. Eng. Comput. 8, 317–332.

di Carlo, A., 1999. A memo of mortar modelling: what could be beyond a bonafide rigid bock-elastic interface models. In: Private Communication to the Authors, Roma.

Eshelby, J.D., 1968a. The elastic behaviour of an elliptical crack. J. Mech. Phys. Solids 17, 177–199.

Eshelby, J.D., 1968b. The elastic field of a crack extending non-uniformly under general anti-plane loading. J. Mech. Phys. Solids 17, 177–199.

Formica, G., Sansalone, V., Casciaro, R., 2003. A mixed strategy for the nonlinear analysis of brick masonry walls. Comput. Meth. Appl. Mech. Eng..

Gambarotta, L., 1995. Stati limite di resistenza per materiali fragili a danneggiamento isotropo. In: Atti del XII congresso nazionale dell'Associazione Italiana di Meccanica Teorica ed Applicata, Napoli.

Gambarotta, L., Lagomarsino, S., 1993. A microcrack damage model for brittle materials. Int. J. Solids Struct. 30 (2), 117–198.

Gambarotta, L., Lagomarsino, S., 1994. Damage in brick masonry shear walls. In: Proc. Europe–US Workshop on Fracture and Damage in Quasi-brittle Structures, Praga.

Gambarotta, L., Lagomarsino, S., 1994. Micromechanically based constitutive equations for concrete-like materials. In: Proc. EURO-C International Conference, Innsbruck, Austria, pp. 223–322.

Gambarotta, L., Lagomarsino, S., Morbiducci, R., 1995. Two-dimensional finite element simulation of a large scale brick masonry wall through a continuum damage model. Internal report.

Hart, V.R., Cundall, P., Lemos, J., 1988. Formulation of a three-dimensional distinct element model—Part ii: Mechanical calculations for motion and interaction of a system composed of many polyhedral blocks. Int. J. Rock Mech., Min. Sci. Geomech. Abstr. 25, 117–126.

Hoenig, A., 1978. The behaviour of a flat elliptical crack in an anisotropic elastic body. Int. J. Solids Struct. 14, 925–934.

Hoenig, A., 1979. Elastic moduli of a non-randomly cracked body. Int. J. Solids Struct. 12, 137–154.

Hughes, Pande (Eds.), 2001. Computer methods in structural masonry—v. In: Proc. STRUMAS V.

Italian Ministry of Public Works, 1981. Instruction for the application of the technical code for the repair and retrofitting of existing buildings damaged by earthquakes. In: Circolare n. 21745.

Kouznetsova, V.G., 2002. Computational homogenization for the multi-scale analysis of multi-phase materials. PhD thesis, Department of Engineering, Technische Universiteit Eindhoven.

Kouznetsova, V.G., Brekelmans, W.A.M., Baaijens, F.P.T., 2001. An approach to micro–macro modeling of heterogeneous materials. Comput. Mech. 27, 37–48.

Kouznetsova, V.G., Geers, M.G.D., Brekelmans, W.A.M., 2002. Multi-scale constitutive modeling of heterogeneous materials with a gradient-enhanced computational homogenization scheme. Int. J. Numer. Meth. Eng. 54, 1235–1260.

Kouznetsova, V.G., Geers, M.G.D., Brekelmans, W.A.M., 2004. Multi-scale second-order computational homogenization of multi-phase materials: a nested finite element solution strategy. Comput. Methods Appl. Mech. Eng.

Krajicinovic, D., 1989. Damage mechanics. In: Mechanics of Materials, vol. 8, p. 117.

Krajicinovic, D., Fonseka, G.U., 1981. The continuous damage theory of brittle materials. J. Appl. Mech. (48), 809–824.

Lagomarsino, S., Gambarotta, L., Morbiducci, R., 1995. Brittle-ductile response of in-plane loaded brick masonry walls. In: Proc. 10th European Europe Conference on Earthquake Engineering, Vienna, pp. 1663–1668.

Lemaitre, J., 1984. How to use the damage mechanics. Nucl. Eng. Des. (80), 233–245.

Lemaitre, J., 1992. A Course on Damage Mechanics. Springer Verlag, Berlin, Germany.

Lourenço, P.B., Rots, J.G., Blaauwendraad, J., 1994. Implementation of an interface cap model for the analysis of masonry. In: de Borst, R., Mang, H., Bicanic, N. (Eds.), Proc. International Conference on Computational Modelling of Concrete Structures, EURO-C, pp. 123–134.

Masiani, R., Rizzi, N.L., Trovalusci, P., 1995. Masonry as structured continuum. Meccanica 30, 673–683.

Massart, T.J., 2003. Multi-scale modeling of damage in masonry structures. PhD thesis, Department of Engineering, Technische Universiteit Eindhoven.

Nemat-Nasser, S., Horii, H., 1983. Overall moduli of solids with microcracks: load-induced anisotropy. J. Mech. Phys. Solids 31 (2), 155–171.
Page, A.W., 1981. The biaxial compressive strength of brick masonry. In: Proc. Inst. Civ. Eng.
Phillips, R., 1998. Multiscale modeling in the mechanics of materials. Curr. Opin. Solid State Mater. Sci. 3, 526–532.
Raijmakers, T.M.J., Vermeltfoort, A.T., 1992. Deformation controlled tests in masonry shear walls. In: Report B-92-1156, TNO-Bouw, Delft, The Netherlands (in Dutch).
Riks, E., 1979. An incremental approach to the solution of snapping and buckling problems. Int. J. Solids Struct. 15, 529–551.
Riks, E., 1984. Bifurcation and stability, a numerical approach. In: WAM Symposium on Innovative Methods for Non-linear Problems, New Orleans.
Salerno, G., de Felice, G., 2000. Continuum modelling of discrete systems: a variational approach. In: Proc. ECCOMAS2000—the Fifth World Congress on Computational Mechanics, Barcellona, 2000.
Salerno, G., Uva, G., 2002. A two-scale algorithm for the nonlinear analysis of damaged masonry brickwork. In: Proc. WCCM V—the Fifth World Congress on Computational Mechanics, Vienna, 2002.
Sanchez Palencia, E., 1992. Introduction aux methodes asymptotique et a l'homogeneisation. Masson.
Suquet, P.M., 1983. Une metode duale en homogenisation: application aux milieux elastiques. J. Mecanique appliquee.
Sutcliffe, D.J., Yu, H.S., Page, A.W., 2001. Lower bound limit analysis of unreinforced masonry shear walls. Comput. Struct. 79, 1295–1312.
Syrmakezis, C.A., Asteris, P.G., 2001. Masonry failure criterion under biaxial stress state. J. Mater. Civil Eng. 13.
Uva, G., 1998. A constitutive model with damage and friction for masonry structures: theoretical and numerical aspects. In: Proc. of the Workshop on Seismic Performance of Monuments Monument-98, Lisbona.